A new and very spiny lizard (Gymnophthalmidae: *Echinosaura*) from the Andes in northwestern Ecuador

Mario H. Yánez-Muñoz [1, 2] , **Omar Torres-Carvajal** [3] , **Juan P. Reyes-Puig** [1, 2] , **Miguel A. Urgiles-Merchán** [1] , **Claudia Koch** [Corresp. 4]

[1] Unidad de Investigación, Instituto Nacional de Biodiversidad (INABIO), Quito, Ecuador

[2] Fundación Red de Protección de Bosques ECOMINGA, Fundación Oscar Efrén Reyes, Departamento de Ambiente, Baños, Ecuador

[3] Museo de Zoología, Escuela de Ciencias Biológicas, Pontificia Universidad Católica del Ecuador, Quito, Ecuador

[4] Herpetology, Zoologisches Forschungsmuseum Alexander Koenig (ZFMK), Bonn, Germany

Corresponding Author: Claudia Koch
Email address: c.koch@zfmk.de

We describe a new species of Neotropical spiny-lizard of the genus *Echinosaura* from the Imbabura and Carchi Provinces on the western slopes of the Andes in northwestern Ecuador. The new species mostly resembles *E. horrida*. However, it can be distinguished from all congeners by having keeled enlarged dorsal scales forming a paired vertebral row, two paravertebral series of short oblique rows of projecting scales, and a pair of spine-like scales on temporal and nuchal regions. We also provide a detailed description of the osteology of the skull and pectoral girdle of the new species and present a phylogenetic hypothesis for *Echinosaura* based on three mitochondrial genes (12S, 16S, ND4) and one nuclear gene (c-mos).

1 **A new and very spiny lizard (Gymnophthalmidae:**
2 ***Echinosaura*) from the Andes in northwestern**
3 **Ecuador**

5 Mario H. Yánez-Muñoz[1,2], Omar Torres-Carvajal[3], Juan P. Reyes-Puig[1,2], Miguel A. Urgiles-
6 Merchán[1], and Claudia Koch[4]*

8 [1] Unidad de Investigación, Instituto Nacional de Biodiversidad (INABIO), Quito, Ecuador.
9 [2] Fundación Red de Protección de Bosques ECOMINGA, Fundación Oscar Efrén Reyes,
10 Departamento de Ambiente, Baños, Ecuador.
11 [3] Museo de Zoología, Escuela de Ciencias Biológicas, Pontificia Universidad Católica del
12 Ecuador, Quito, Ecuador.
13 [4] Herpetology, Zoologisches Forschungsmuseum Alexander Koenig (ZFMK), Bonn, Germany.

15 *Corresponding Author:
16 Claudia Koch[4]
17 Email address: c.koch@leibniz-zfmk.de

Abstract

20 We describe a new species of Neotropical spiny-lizard of the genus *Echinosaura* from the
21 Imbabura and Carchi Provinces on the western slopes of the Andes in northwestern Ecuador. The
22 new species mostly resembles *E. horrida*. However, it can be distinguished from all congeners
23 by having keeled enlarged dorsal scales forming a paired vertebral row, two paravertebral series
24 of short oblique rows of projecting scales, and a pair of spine-like scales on temporal and nuchal
25 regions.

27 We also provide a detailed description of the osteology of the skull and pectoral girdle of the
28 new species and present a phylogenetic hypothesis for *Echinosaura* based on three mitochondrial
29 genes (12S, 16S, ND4) and one nuclear gene (c-mos).

Introduction

33 Neotropical spiny-lizards traditionally ranked as the genus *Echinosaura* Boulenger 1890 are
34 small riparian lizards occuring west of the Andes from Panama to Ecuador (*Vásquez-Restrepo et*
35 *al., 2020*). Most species of *Echinosaura* have partially compressed tails and bear enlarged
36 tubercles and strongly keeled scales on body and tail, often forming crests, which represent
37 adaptations for aquatic locomotion (*Marques-Souza et al., 2018*).

39   Recent molecular phylogenetic studies have resulted in major taxonomic changes within
40   *Echinosaura*, such as synonymy of *Teuchocercus* Fritts & Smith 1969 with *Echinosaura* and
41   description of *Centrosaura* Uzzell 1966 and *Rheosaurus* Vásquez-Restrepo, Ibáñez, Sánchez-
42   Pacheco & Daza 2020, to accommodate *"E. apodema"* Uzzell 1966 and *"E. sulcarostrum"*
43   Donnelly, Macculloch, Ugarte & Kizirian 2006, respectively (*Torres-Carvajal et al., 2016*;
44   *Vásquez-Restrepo et al., 2020*).
45   Of the seven currently recognized species of *Echinosaura*, four are known from Ecuador: *E.*
46   *brachycephala*, *E. horrida*, *E. keyi* and *E. orcesi,* all from western humid tropical and subtropical
47   areas (*Torres-Carvajal et al., 2021*).
48
49   In extreme northwestern Ecuador, specifically in Carchi province near the national border with
50   Colombia, important remnants of native vegetation are still preserved due to inaccessibility and
51   local conservation initiatives. During the last six years, we have focused on the study and
52   conservation of this important biodiversity area, discovering several new species and many
53   candidate species of small vertebrates that are still awaiting formal description (*Yánez-Muñoz et*
54   *al., 2018; Reyes-Puig et al., 2020; Brito et al., 2020*). Here, we describe a new species of
55   *Echinosaura* recognized and delimited by a molecular phylogenetic analysis along with several
56   types of morphological evidence, including cranial osteology. Accordingly, the first detailed
57   description of the cranial morphology of *Echinosaura* based on CT scan data of the new species
58   is presented.
59
60
61   **Materials and Methods**
62   **Ethics statement.** We conducted this study under research permits MAE-DNB-CM-2016-0045
63   and MAE-DNB-CM-2019-0120, issued by the Ministerio del Ambiente del Ecuador. We
64   followed the guidelines for use of live amphibians and reptiles in field research (*Beaupre et al.,*
65   *2004*), compiled by the American Society of Ichthyologists and Herpetologists, the
66   Herpetologists' League and the Society for the Study of Amphibians and Reptiles.
67
68   **Taxon sampling.** We examined 36 specimens of *Echinosaura* (Appendix) housed in the
69   following collections: División de Herpetología del Instituto Nacional de Biodiversidad
70   (DHMECN), Quito, Ecuador; Museo de Zoología de la Pontificia Universidad Católica del
71   Ecuador (QCAZ), Quito, Ecuador; Natural History Museum (BMNH), London, UK; University
72   of Illinois Museum of Natural History (UIMNH), Illinois, USA; Muséum d'Histoire Naturelle de
73   la Ville de Genève (MHNG), Geneva, Switzerland; Natural History Museum Vienna (NMW),
74   Vienna, Austria; Zoological Research Museum Alexander Koenig (ZFMK), Bonn, Germany. We
75   mapped locality records using ArcMap 10.5.1 (ESRI, Inc.) with a WGS84 datum and Universal
76   Transverse Mercator conformal projection.
77
77   We adopted the unified species concept (*de Queiroz, 2007*) by considering different lines of
78   evidence (e.g., external morphology, osteology, hemipenial morphology, molecular phylogeny)

79   as species delimitation criteria. We considered monophyly as additional evidence for recognizing
80   populations as new species. The electronic version of this article in Portable Document Format
81   (PDF) will represent a published work according to the International Commission on Zoological
82   Nomenclature (ICZN), and hence the new names contained in the electronic version are
83   effectively published under that Code from the electronic edition alone. This published work and
84   the nomenclatural acts it contains have been registered in ZooBank, the online registration
85   system for the ICZN. The ZooBank LSIDs (Life Science Identifiers) can be resolved, and the
86   associated information viewed through any standard web browser by appending the LSID to the
87   prefix http://zoobank.org/. The LSID for this publication is:
88   urn:lsid:zoobank.org:pub:9D513A0D-D676-4290-AE5D-A128B7DBE3F3.

89

90   **Field work.** We conducted field work in the foothill forests of Carchi province associated with
91   several small river basins during a joint expedition of Instituto Nacional de Biodiversidad
92   (INABIO) and Ecominga Foundation in three sectors of the Dracula Reserve: (1) Río Pailón
93   Chico (0.982, -78.233; 1,224 m), 6–11 November 2017 and 19–25 August 2018; (2) Guapilal
94   (0.891, -78.203; 1,640–1,750 m), 22–26 April 2019; (3) Cerro Oscuro (0.886, -78.190; 1,600 m),
95   4–6 July 2020; and (4) Bosque Comunal La Esperanza (0.954, -78.237; 1,439–1,623 m), 22–31
96   March 2021. We collected the specimens using visual encounter surveys and pitfall traps
97   (*Fitzgerald, 2012*) and after photographing them alive, we euthanized the animals with
98   benzocaine, extracted a sample of muscle tissue from each individual and preserved the samples
99   in 95% ethanol. Subsequently, we fixed the specimens in 10% formalin, and preserved in 75%
100 ethanol.

101 **Morphological data and analysis.** Following *Vásquez-Restrepo et al. (2020)*, we recorded the
102 following 12 morphometric characters with a digital caliper (Trupper, precision ±0.01 mm,
103 rounded to 0.1 mm) using a 10x Boeco BS-80 stereo microscope: snout–vent length (SVL),
104 measured from tip of snout to cloacal opening; trunk length (TRL), measured longitudinally from
105 axilla to groin; tail length (TAL), measured from cloacal opening to tip of tail; snout length (SL),
106 measured from tip of snout to anterior edge of eye; head length (HL), measured from tip of snout
107 to anterior edge of tympanum; head width (HW), measured at level of greatest width; humerus
108 length (HUM), measured from edge of joint to edge of shoulder; forearm length (FAL),
109 measured from edge of joint to base of hand; hand length (HND), measured from base of hand to
110 tip of fourth finger; femur length (FEM), measured from groin to outer edge of knee; tibia length
111 (TIB), measured from outer edge of knee to base of foot; foot length (FTL), measured from base
112 of foot to tip of fourth toe. Except for males with everted hemipenes, we determined the sex by
113 subcaudal incision, or by secondary sexual characteristics like the number of femoral pores. We
114 used the terminology proposed by *Fritts, Almendáriz & Samec (2002)*, *Köhler, Böhme & Schmitz
115 (2004)*, and *Vásquez-Restrepo et al. (2020)* for scale characters and measurements. We obtained
116 data of color in life from field notes and photographs.

117 We extracted the right hemipenis of the male holotype (DHMECN 15208) from the recently
118 collected specimenand then filled the extracted organ with blue-stained petroleum jelly and
119 immersed it in a solution of alizarin red for two hours. Thereafter we washed the hemipenis to

120 remove excess alizarin red and finally transferred to 70% ethanol. Terminology for hemipenial
121 structures follows *Uzzell (1973)*, *Savage (1997)* and *Nunes et al. (2012)*.

122 We obtained information on skeletal morphology and stomach contents from two specimens of
123 the new species (DHMECN 15210, DHMECN 15208) by use of an X-ray in 2D (Faxitron X-ray
124 LX60) and a micro-CT scanner (Bruker SkyScan 1173) in 3D, both devices available at ZFMK.
125 We placed the specimens in a plastic container and mounted it on styrofoam to avoid movements
126 during scanning. We CT-scanned the specimens in 180° degrees using rotation steps of 0.3°
127 degrees with a tube voltage of 35 kV and a tube current of 150 uA, without the use of a filter, at
128 an image resolution of 39.3 μm. Scan duration was 30 min with an exposure time of 280 ms. We
129 reconstructed the CT-datasets using N-Recon software (Bruker MicroCT) and rendered both
130 scans in three dimensions with the program CTVox version 2.6 (Bruker MicroCT). Additionally,
131 we rendered and segmented the skull of a female paratype (DHMECN 15210) in three
132 dimensions to separate and color individual bones through the aid of Amira visualization
133 software (FEI, Thermo Fisher Scientific). We provide a detailed description of the skull,
134 vertebrae and pectoral girdle based on data of the female paratype (DHMECN 15210). We
135 omitted cartilage structures because micro-CT does not render cartilage. Osteological
136 terminology follows *Evans (2008)*, *Jerez & Tarazona (2009)*, *Roscito & Rodrigues (2010)*,
137 *Rodrigues et al. (2013)*, and *Hernández Morales et al. (2019)*.

138

139 **DNA sequence data and phylogenetic analyses.** We digested and extracted total genomic DNA
140 from liver or muscle tissue using a guanidinium isothiocyanate extraction protocol. Using
141 primers and amplification protocols from the literature (*Torres-Carvajal et al., 2016*), we
142 generated DNA sequences of mitochondrial genes 12S, 16S, and ND4, as well as nuclear gene c-
143 mos from two individuals of the new species described herein (GenBank accession numbers
144 [DHMECN 14058 and 15208, respectively] MW525208–09 [12S], MW525211–12 [16S],
145 MW512698–699 [ND4], and MW512700–701 [c-mos]). We retrieved all available GenBank
146 sequences of these genes for other *Echinosaura* species, as well one sample per species of all
147 clades ranked as genera within Cercosaurinae including "unnamed" clades (*Torres-Carvajal et
148 al., 2016*).

149

150 We aligned DNA sequences using MAFFT (*Katoh & Standley, 2013*) under default settings in
151 Geneious Prime 2020.2.2 (https://www.geneious.com), and translated ND4 and c-mos sequences
152 into amino acids for confirmation of alignment. Our final concatenated data matrix contained
153 148 taxa and 1,935 characters and was partitioned by gene and codon position (i.e., eight
154 partitions total). We chose the best partitioning scheme using PartitionFinder v2.1.1 under the
155 Bayesian Information Criterion (BIC), and the ″greedy″ algorithm with branch lengths of
156 alternative partitions ″linked″ to search for the best-fit scheme (*Guindon et al., 2010; Lanfear et
157 al., 2012; Lanfear et al., 2017*). We combined the genes into a single dataset with six partitions:
158 (i) 12S, 16S [GTR + I + G]; (ii) 1st codon position of ND4 [GTR + I + G]; (iii) 2nd codon
159 position of ND4 [GTR + I + G]; (iv) 3rd codon position of ND4 [GTR + G]; (v) 3rd codon
160 position of c-mos [K80 + G]; and (vi) 1st and 2nd codon positions of c-mos [HKY + G]. We run

161   a maximum likelihood analysis in RAxML v8.2.10 (*Stamatakis, 2014*) under the GTRGAMMA
162   model, while we assessed nodal support with the rapid bootstrapping (BS) algorithm
163   (*Stamatakis, Hoover & Rougemont, 2008*) on 1,000 replicates. We run a Bayesian analysis in
164   MrBayes v3.2.7 (*Ronquist et al., 2012*), with all parameters unlinked between partitions (except
165   topology and branch lengths) and rate variation (prset ratepr = variable) invoked. We set four
166   independent runs, each with four MCMC chains, for 107 generations, sampling every 10,000
167   generations. We calculated posterior probabilities (PP) on a Maximum Clade Credibility Tree in
168   TreeAnnotator (*Rambaut & Drummond, 2016*) and rooted the trees with *Alopoglossus* (*Castoe,*
169   *Doan & Parkinson, 2004*; *Goicoechea et al., 2016*; *Pellegrino et al., 2001*). We executed
170   phylogenetic analyses in the CIPRES Science Gateway (*Miller, Pfeiffer & Schwartz, 2010*). In
171   addition, we calculated pairwise genetic distances for ND4 and 16S genes among species of
172   *Echinosaura* using DIVEIN (*Deng et al., 2010*).
173

174   **Results**
175

176   **Phylogenetic relationships.** Maximum likelihood and Bayesian analyses resulted in nearly
177   identical topologies (Fig. 1). Both analyses support monophyly of the new species of
178   *Echinosaura* described in this paper. The monophyly of *Echinosaura* is maximally supported
179   (BS = 100, PP = 1). There is a basal split into two clades, one of which (BS = 96, PP = 1)
180   contains *E. orcesi* as sister to (*E. panamensis*, (*E. centralis*, *E. palmeri*)). The second clade (BS =
181   53, PP = 1) includes, following branching order, *E. keyi*, *E. brachycephala* (sister to *E. keyi* in
182   the ML tree), and the new species described below as sister to *E. horrida* with strong support
183   (BS = 98, PP = 1). Uncorrected pairwise genetic distances for ND4 between *Echinosaura* sp.
184   nov. and other congenerics range between 0.20, with both *E. horrida* and *E. keyi*, and 0.35 with
185   *E. centralis*. Distances for 16S range from 0.06 with *E. brachycephala* to 0.14 with *E.*
186   *panamensis*.
187

188   **Systematic accounts**

189   **Squamata** Oppel, 1811
190

191   **Gymnophthalmidae** Merrem, 1820
192

193   *Echinosaura* Boulenger, 1890
194

195   *Echinosaura fischerorum* **sp. nov.**
196   LSID: urn:lsid:zoobank.org:act:F8DCFE99-4862-4476-9A5C-EB684D0CD73A
197

198   **Proposed standard Spanish name:** Lagartijas espinosas de los Fischer
199   **Proposed standard English name:** Fischers' Spiny Lizards

200

Holotype (Figs. 2, 3, 4, 5, 6, 7). DHMECN 15208, adult male, from Reserva Dracula, Sector El Guapilal (0.891, -78.203; 1,689 m), Carchi Province, Ecuador, collected on 22 April 2019 by Juan P. Reyes-Puig, Daniela Franco and Héctor Yela.

204

Paratypes (Figs. 4, 5, 6, 8, 9, 10). DHMECN 15209 and DHMECN 15211, adult males, DHMECN 15210, adult female, all with same data as holotype; DHMECN 14058 and DHMECN 14060, adult females, DHMECN 14059 and DHMECN 14061, juvenile females, all from Reserva Dracula, Sector El Pailón Chico (0.983, -78.296; 1,495 m), collected on 8 November 2017 by Mario H. Yanez-Muñoz, Juan P. Reyes-Puig and Fausto Recalde; DHMECN 12767, juvenile female from Cerro Oscuro, Reserva Dracula (0.886, -78.190; 1,600 m) collected on June 2015 by Héctor Yela; DHMECN 16109, adult female and DHMECN 16110, adult male, from Comunidad La Esperanza (0.954, -78.237; 1,623 m), collected on 28 March 2021 by Mario H. Yánez-Muñoz, Juan P. Reyes-Puig and Miguel A. Urgiles-Merchán.

214

Diagnosis. The new species can be distinguished from all congeners by the combination of the following characteristics: 1) snout pointed; 2) internasal single; 3) frontonasals paired; 4) frontal single; 5) frontoparietal paired; 6) supraoculars three, large; 7) supralabials five; 8) infralabials four; 9) postmental single; 10) chin shields enlarged, in one pair; 11) dorsum with a vertebral row of paired, enlarged, keeled scales; 12) two paravertebral series of short oblique rows of projecting scales, with scales increasing in size posteriorly on each row so that the most posterior scale of each row is a greatly enlarged, projecting spine; 13) spiny scales forming oblique lines on body flanks; 14) ventral scales squared, keeled; 15) subdigital lamellae on fourth finger 14–18; 16) subdigital lamellae on fourth toe 24–27; 17) femoral pores per hind limb in males 7–9; 18) dorsal surface of tail with two longitudinal rows of enlarged keeled scales that are more conspicuous on the anterior half of tail; 19) subcaudals per caudal segment three (anterior third of tail excluded); 20) tip of snout with creamy orange marks; 21) dorsal background dark brown with creamy orange paravertebral blotches extending onto anterior end of tail; 22) intense orange nuchal spines; 23) base of tail dorsally with a pair of pale orange blotches; 24) venter gray, marmorated with black and dark brown; 25) femoral pores yellowish cream; 26) premaxillary tooth loci 11–12; 27) maxillary tooth loci 17–18; 28) dentary tooth loci 22–23; 29) nasal bones in medial contact along most of their length; 30) postfrontal expands posteriorly to form part of the anterior border of the supratemporal fenestra.

233

Comparison with similar species (Figs. 11, 12, 13, 14). *Echinosaura fischerorum* sp. nov. differs from all *Echinosaura* species in having keeled enlarged dorsal scales forming a paired vertebral row, two paravertebral series of short oblique rows of projecting scales, and a pair of spine-like scales on each side in temporal and nuchal region (see Table 1).

Echinosaura fischerorum sp. nov. most closely resembles *E. horrida* (character states in parentheses), but can be distinguished from this species in having a wide postmental in contact

240 with anterior 3/4 of first infralabial (Fig. 3C; postmental longer than wide, in contact with first
241 and second infralabials); keeled (smooth) enlarged dorsal scales forming a paired vertebral row;
242 scales on each side of vertebral row heterogeneous in size (granular, homogeneous in size), with
243 enlarged scales forming chevrons (Fig. 12A, B); sharp (blunt) spiny scales throughout body,
244 forearms and legs; striated (smooth) dorsal and lateral head scales; keeled (smooth) parietals;
245 nasal bones in medial contact along most of their length (distinctly separated, resulting in contact
246 between premaxilla and frontal bone); postfrontal bone expands posteriorly to form part of the
247 anterior border of the supratemporal fenestra (postfrontal excluded from the supratemporal
248 fenestra by contact of postorbital with parietal). Although our sampling size is small, *E.*
249 *fischerorum* sp. nov. seems to be smaller (maximum SVL = 68 mm) than *E. horrida* (maximum
250 SVL = 86 mm).

251

252 **Description of adult male holotype (Figs. 2, 3)**. Rostral single, in contact with internasal
253 posteriorly, nasals and first supralabials posterolaterally; internasal single, wider than long,
254 rugose, in contact with rostral anteriorly, nasals laterally, and frontonasals posteriorly; nasals
255 pentagonal, in contact with rostral anteriorly, internasal and frontonasal dorsally, frenocular and
256 lorilabial posteriorly, and first supralabial ventrally; frontonasals paired, rugose, nearly
257 rectangular and twice as long as wide, with posterior edges forming an obtuse angle, in contact
258 with internasal anteriorly, pre-supraocular scales and frontal posteriorly, and nasal and frenocular
259 ventrally; frontal single, rugose, subpentagonal, wider than long, in contact with frontonasals
260 anteriorly, pre-supraocular scales and first supraocular scales laterally, and frontoparietals
261 posteriorly; supraoculars three; first supraocular larger than others, in contact with frontal and
262 pre-supraocular scales anteriorly, frontoparietal medially, supercilliaries laterally, and second
263 supraoccipital posteriorly; lower eyelid with unpigmented palpebral disc divided into three large
264 scales; frenocular large, rectangular, about twice as long as tall, in contact with nasal anteriorly,
265 frontonasal dorsally, lorilabial ventrally, preoculars and first pre-supraocular posteriorly;
266 lorilabial in contact with nasal anteriorly, first and second supralabials ventrally, frenocular and
267 preoculars dorsally, and first subocular posteriorly; suboculars in 2–5 longitudinal rows, of
268 which the ventralmost contains five enlarged scales in contact with supralabials III–V;
269 frontoparietals two, similar in size to frontal when combined, contacting frontal anteriorly, first
270 and second supraocular laterally, and scales of parietal region posteriorly; parietal region covered
271 with small irregular scales; one pair of spine-like temporals on each side; supralabials five;
272 infralabials four; mental longer than wide, in contact with postmental posteriorly and first
273 infralabials laterally; postmental trapezoidal, in contact with first infralabials laterally and one
274 pair of chin shields and two small lateral scales posteriorly; chin shields in one pair, about twice
275 as long as wide, separated from infralabials by small scales; gular region with five transverse
276 rows of 5–7 large spiny scales that extend to lower part of tympanum.

277 Dorsum with a vertebral row of paired, enlarged, keeled scales, and two paravertebral series of
278 short oblique rows of projecting scales, with scales increasing in size posteriorly on each row so
279 that the most posterior scale forms a greatly enlarged, projecting spine; scales between vertebral
280 row and paravertebral series of short rows heterogeneous in size, with enlarged scales forming

281 oblique rows that converge medially to form chevrons; body flanks with seven oblique rows of
282 spine-like scales, which are separated from each other by small, irregular, tubercular scales;
283 ventral scales keeled, with rounded edges and in four longitudinal rows on pectoral region, but
284 squared and in eight longitudinal rows on belly.

285 Limbs pentadactyl; digits clawed; subdigital lamellae on fourth finger single (second subdigital
286 on left side divided), 16 on left side and 14 on right side; subdigital lamellae on fourth toe 24 on
287 both sides; dorsal surface of tail with two longitudinal rows of enlarged keeled scales in five to
288 six pairs per caudal segment, increasing in size posteriorly on each segment; caudal longitudinal
289 rows separated from each other by 3–7 small scales; four pairs of subcaudals per autotomic
290 segment on anterior third of tail; three pairs of subcaudals per autotomic segment on posterior
291 two thirds.

292 **Coloration of holotype in life (Fig. 6A).** The holotype has a dark brown dorsal background with
293 creamy orange paravertebral blotches extending onto anterior end of tail; flanks with grayish
294 cream circular marks; parietal region brown orange; temporal region and posterior border of
295 mandible with scattered white scales; tip of snout with creamy orange marks; first supraocular
296 with diagonal grayish cream line; supercilliaries with 2–3 pale marks; supralabials with a pair of
297 grayish cream bars; nuchal spines intense orange; some spines along paravertebral rows creamy
298 orange; dorsally, the base of the tail with a pair of pale orange blotches; venter gray, marmorated
299 with black and dark brown; femoral pores yellowish cream; round, cream blotch on supra-anal
300 region; limbs dark brown with grayish cream marks; iris copper red.

301 **Coloration of holotype after 1-5 years in preservative (Figs. 2, 4, 5).** The holotype is dorsally
302 brown, with six pairs of paravertebral cream blotches; base of tail with broad transverse,
303 yellowish cream bar; tip of snout with cream nasal and internasal scales; lips and chin with
304 cream bands separated by black interspaces; ventral surface of body and limbs dark brown with
305 cream marbling; femoral pores pale gray.

306

307 **Measurements of the holotype (in mm).** SVL = 69 mm; TAL = 89.5 mm; TRL = 33.6 mm; SL
308 = 13.7 mm; HL = 20.1 mm; HW = 13.2 mm; HUM = 9.7 mm; FAL = 9.1 mm; HND = 9.3 mm;
309 FEM = 12.5 mm; TIB = 13.7 mm; FTL = 15.7 mm

310

311 **Variation (Figs. 4, 5, 6).** Intraspecific variation in morphometrics and lepidosis is presented in
312 Tables 2 and 3. After 1-5 years in preservative (Figs. 4, 5), the paravertebral cream blotches of
313 some male specimens are merged, sometimes forming continuous paravertebral stripes
314 (DHMECN 15211); in females, both the paravertebral blotches and the dorsal transverse bar on
315 base of tail are faint (DHMECN 14058) or absent (DHMECN 14060), whereas juveniles have a
316 pair of light paravertebral stripes (DHMECN 14061) or a broad vertebral stripe along dorsum
317 (DHMECN 12767, 14059), with a conspicuous dorsal transverse bar on base of tail. Regardless
318 of sex or age, the snout (rostral, internasal and prefrontal scales) varies between cream, orange
319 cream, and dark brown; gular background varies from dark brown to reddish brown; coloration

320   of the belly can be predominantly dark brown. In life, the dorsal pale spots vary from yellowish
321   cream to orange cream (Fig. 6).

322

323   **Hemipenes (Fig. 7).** The lobes of the expanded, heart-shaped right hemipenis, are not fully
324   everted; it is 9.2 mm long and 8.7 mm wide. It has a globular hemipenial body, thinner at the
325   base and broader distally, and bears two small symmetrical lobes. The sulcus spermaticus is
326   defined by two thick parallel margins and extends medially in a straight line along the
327   hemipenial body up to the lobular crotch, where a fleshy fold divides it into two branches that
328   run medially on each lobe. Five short, oblique, and parallel flounces bearing five to seven
329   calcified spicules each lie on each side of the sulcus spermaticus with a narrow nude area in
330   between. Lateral and asulcate aspects of hemipenis are ornamented distally with eight
331   approximately equidistant flounces bearing rows of calcified spicules; of these, the five distal
332   flounces converge on the asulcate face forming chevrons with apices directed toward base of
333   hemipenis, while the other three flounces increasingly diverge toward base of organ. On the
334   asulcate side, these flounces are separated medially by a large naked region. Ventral to the
335   flounces, the lateral and asulcate sides of the hemipenial body are covered by 41 large, evenly
336   distributed spines that increase slightly in size towards the base of the organ.

337

338   **Cranial Osteology (Figs. 8, 9, 10).** The following description of the skull of *Echinosaura*
339   *fischerorum* sp. nov. is based on female paratype DHMECN 15210. The skull is robust,
340   moderately compressed (skull width = 60% of skull length) and moderately high (skull height =
341   43% of skull length). The widest region of the skull is at the level of the contact between
342   squamosal and jugal. The dorsal margin of the snout in lateral view is slightly convex. The
343   surface of frontal and parietal is very rugose. Basioccipital, compound otooccipitals (fused
344   opisthotic and exoccipital), prootics and supraoccipital are almost indistinguishably fused and the
345   parabasisphenoid is partly fused to this structure. The mandibles are very robust, and coronoid,
346   splenial and angular are largely fused with the compound bone. Intraspecific variation in cranial
347   osteology of *Echinosaura fischerorum* sp. nov. is presented in Figs. S1 and S2.

348

349   *Dermatocranium*
350   **Premaxilla (Figs. 8, 9A).** The premaxilla bears 12 tooth loci. The ascending nasal process of the
351   premaxilla contacts the nasals posteriorly and forms the anterior and the anterodorsal edge of the
352   naris laterally. There is a small foramen anterolaterally on both sides of the premaxilla. The
353   palatal shelf of the premaxilla is notched medially and contacts the premaxillary process of the
354   maxilla.

355

356   **Maxilla (Figs. 8, 9A).** The maxilla bears 18 tooth loci, arranged in a straight row. The bone is
357   large and occupies most of the lateral surface of the skull anterior and ventral to the orbit. The
358   anterolateral process of the maxilla is slightly notched anteriorly and articulates with the
359   maxillary process of the premaxilla. The facial process of the maxilla is triangular and forms the
360   posterior edge of the naris. It contacts the nasal and the frontal dorsally, and the prefrontal

361   posterodorsally, extensively overlapping the anterior process of the prefrontal. There is a row of
362   five foramina on the supralabial edge of the facial process. The posterolateral process of the
363   maxilla is posteriorly bifurcate and articulates with the jugal. The anteromedial process of the
364   maxilla is elongate, triangular, and contacts the palatal shelf of the premaxilla laterally and the
365   vomer medially, which represents the only contact point between the maxilla and the vomer. The
366   medial edge of the palatal shelf of the maxilla is irregularly shaped and broadest at the level of
367   maxillary teeth 7–10, tapering abruptly posterior to tooth 10 and ending at the level of tooth 14.
368   It forms a palatine facet, where the palatine articulates at the level of maxillary teeth 11–13. The
369   posteromedial process of the maxilla articulates with the maxillary process of the ectopterygoid.
370
371   **Nasal (Figs. 8A, C, 9A).** The nasal is ellipsoid in dorsal view, much longer than wide and about
372   twice as long as the premaxilla. Along the anterior half of the nasal its lateral edge articulates
373   with the dorsal edge of the naris and along its posterior half it contacts the facial process of the
374   maxilla laterally. Anteriorly the nasal is convexly shaped and in broad contact with the
375   premaxilla. Both nasals are in broad contact medially. Posteriorly the nasal is in broad contact
376   with the frontal.
377
378   **Frontal (Figs. 8, 9).** The anterior margin of the frontal is less than half the width of its posterior
379   edge. The interorbital constriction is distinctly narrower than the anterior edge and at its
380   narrowest point about one fourth the width of the posterior edge. The anterior margin has three
381   pointed processes in dorsal view, of which the lateral two are slightly longer than the medial
382   process. The nasal facets of the frontal are between the medial process and the lateral processes.
383   The lateral process of the anterior margin contacts the dorsal edge of the facial process of the
384   maxilla. The lateral margin of the frontal contacts the posterodorsal process of the prefrontal
385   anteriorly and the anterior half of the dorsal edge of the postfrontal posteriorly. The median part
386   of the frontal (posterior to the contact zone with the prefrontal and anterior to the contact zone
387   with the postfrontal) is part of the dorsal margin of the orbit. The posterior edge of the frontal has
388   a pair of short frontoparietal tabs (*Roscito & Rodrigues, 2010*) that project slightly and articulate
389   with the frontal facets of the parietal. The cristae cranii originate on the ventrolateral surface of
390   the frontal and meet each other at midline, where they are fused into a tubular structure that
391   extends posteriorly almost to the level where the anterior tip of the postfrontal contacts the
392   frontal. This structure encapsulates the olfactory tract and reaches anteriorly to the level of the
393   nasals. The anterolateral border of the cristae cranii contacts the medial edge of the prefrontal.
394
395   **Parietal (Figs. 8, 9).** The parietal is about as long as wide. It is distinctly shorter than the frontal
396   and its widest part is narrower than the posterior end of the frontal. The anterolateral and the
397   posterolateral processes of the parietal taper distally and are oriented outwards. The anterolateral
398   process extends into the suture between the frontal and the postfrontal, which is the only contact
399   zone between the parietal and postfrontal. The posterolateral process contacts the supratemporal
400   and the squamosal posterolaterally, and the paroccipital process of the otoccipital posteriorly.

401   The posterior edge of the parietal bears a posteromedial notch. The lateral margin of the parietal
402   posterior to the anterolateral process forms the dorsal margin of the supratemporal fenestra. A
403   slender post-temporal fenestra is present, delimited anteriorly by the posterior margin of the
404   parietal, and posteriorly by the supraoccipital, separated at the midline by a short anterior
405   projection of the supraoccipital. On the ventral side of the parietal, a triangular descending
406   process originates anterolaterally just posterior to the anterolateral process; the triangular process
407   lies medial to the epipterygoid and reaches its dorsal tip without contact. The descending process
408   lies slighty anterior to the alar process of the prootic.
409

410   **Prefrontal (Fig. 8A, C).** The prefrontal forms the anterior and anterodorsal margins of the orbit.
411   The orbitonasal flange of the prefrontal contacts medially the anterolateral surface of the cristae
412   cranii of the frontal and the anterior border of the palatine. A lacrimal foramen is present
413   between the internal wall of the facial process of the maxilla and the ventral process of the
414   prefrontal that rests half on the maxillary palatal shelf and half of the palatine. The ventral
415   process of the prefrontral is broadly separated from the anterior process of the jugal. The
416   posterodorsal process of the prefrontal is placed beneath the lateral margin of the frontal and is,
417   thus, not visible in dorsal view.
418

419   **Postfrontal (Figs. 8, 9).** The postfrontal is triradiate and forms part of the posterodorsal margin
420   of the orbit, contacting dorsally the posterior part of the frontal and the anterior part of the
421   parietal. The ventral process of the postfrontal contacts the jugal ventrally, forming the
422   postorbital bar and excluding the postorbital from the orbit. Laterally, the postfrontal contacts the
423   postorbital. The posterodorsal process of the postfrontal comprises more than half the total length
424   of the postfrontal and expands posteriorly to form part of the anterior border of the
425   supratemporal fenestra. The acute anterior process of the postfrontal is triangular, projecting
426   anteromedially, and corresponds to two-thirds of the length of the posterodorsal process.
427

428   **Postorbital (Figs. 8, 9).** The postorbital is long and lozenge-shaped. Anteriorly and along the
429   anterior half of its dorsal margin it contacts the postfrontal. The posterior half of its dorsal
430   margin forms the lateral border of the supratemporal fenestra. It contacts the dorsal surface of the
431   anterior half of the squamosal posteriorly.
432

433   **Squamosal (Figs. 8, 9).** The squamosal is long and has a hockey-stick shape. The anterior two-
434   thirds are straight and taper into an acute tip, contacting the postorbital dorsally and the
435   posterodorsal ending of the jugal laterally. The posterior part curves downwards to meet the
436   supratemporal medially. The posteroventral tip fits into the deep notch of the tympanic crest of
437   the quadrate. The squamosal forms the posterolateral border of the supratemporal fenestra and
438   the posterodorsal border of the infratemporal fenestra.
439

440 **Epipterygoid (Figs. 8C, 9A).** The epipterygoid is a rod-like slender bone with slightly expanded
441 epiphyses. The ventral epiphysis inserts into the fossa columellae of the pterygoid, and the dorsal
442 epiphysis is located anterior to the alar process of the prootic and lateral to the descending
443 process of the parietal, but not contacting these elements.

445 **Supratemporal (Figs. 8A, C, 9B).** The supratemporal is a small, rod-like slender bone which
446 contacts the posterolateral process of the parietal dorsally, the squamosal laterally, the
447 paroccipital process of the otoccipital medially, and the quadrate ventrally.

449 **Quadrate (Figs. 8, 9).** The quadrate is robust and conchal-shaped. It can be divided into a
450 ventrally located mandibular condyle, articulating with the compound bone of the mandible, and
451 a dorsally located cephalic condyle articulating with the supratemporal, the paroccipital process
452 of the prootic and the ventral tip of the squamosal, which fits into a deep notch in the dorsal
453 surface of the quadrate. A lateral concave tympanic crest, a posterior crest and a medial crest
454 extend between the mandibular and cephalic condyles.

456 **Jugal (Figs. 8, 9).** The jugal is sigmoidal in shape. It forms part of the ventral and the posterior
457 margins of the orbit. Anteriorly it is bifurcated with a longer pointed suborbital process and a
458 shorter more rounded maxillary process. The robust dorsal temporal process contacts the ventral
459 margin of the postfrontal, the postorbital and the anterior process of the squamosal, where it ends
460 in a blunt tip. Medially, the jugal has a triangular ectopterygoid process, which contacts the
461 lateral margin of the ectopterygoid. On its lower edge the jugal has a long and robust triangular
462 free posterior process.

464 **Vomer (Fig. 8B).** The elongate vomer is the most anterior component of the skull floor located
465 posterior to the premaxillary palatal shelf and attached to a cavity in it. The anterior process
466 tapers to a pointed tip. The lateral shelf of the vomer has an irregular border that partly overlaps
467 the palatal shelf of the maxilla dorsally. There is an anterolateral process that overlaps the
468 vomeronasal fenestrae without contacting the maxillary palatal shelf. Posteriorly, the slender
469 palatine process of the vomer overlaps ventrally the vomerine process of the palatine. The dorsal
470 surface of the vomer has a curved transversal crest that contacts the septomaxilla. Posterior to the
471 crest is a large vomerine foramen. There is a dorsal crest along the medial border of the vomer,
472 which contacts its counterpart on the other vomer.

474 **Palatine (Fig. 8).** The palatine forms the middle portion of the skull floor. It is anteriorly wider
475 and narrows posteriorly to meet the pterygoid. Anteromedially, the vomerine process overlaps
476 the posterior end of the vomer. Anterolaterally, the wide maxillary process of the palatine
477 articulates with the maxillary palatal shelf. Between the medial and lateral extremities of its
478 anterior margin the palatine has a ventral concave surface, deeper anteriorly and gradually
479 shallower posteriorly, which forms the choanal channel. Posteriorly, the pterygoid process

480   overlaps dorsally the medial palatine process of the pterygoid. The lateral margin of the posterior
481   part of the palatine forms the medial margin of the suborbital fenestra.

482

483   **Pterygoid (Figs. 8, 9).** The Y-shaped pterygoid forms the posterior part of the skull floor.
484   Anteriorly, the pterygoid is divided into a medial lanceolate palatine process and a lateral
485   triangular and broad ectopterygoid process, forming the posterior margin of the suborbital
486   fenestra. The palatine process overlaps with the pterygoid process of the palatine. The
487   ectopterygoid process fits into a facet between the dorsal and ventral portions of the
488   posteromedial process of the ectopterygoid. Posteriorly, the long and slender quadrate process
489   extends dorsolaterally to almost reach, but not contact the medial crest of the quadrate. The
490   basipterygoid process of the parabasisphenoid contacts the pterygoid medially at about
491   midlength. The dorsomedial surface of the pterygoid has a shallow groove, the fossa columellae,
492   into which the ventral epiphysis of the epipterygoid inserts.

493

494   **Ectopterygoid (Fig. 8B, C).** The ectopterygoid is a short but robust bone that forms part of the
495   posterior and external margin of the suborbital fenestra. Anteriorly, its maxillary process
496   articulates with the posteromedial process of the maxilla. Laterally, it contacts the triangular
497   ectopterygoid process of the jugal. Posteriorly, the posteromedial process of the ectopterygoid
498   articulates with the ectopterygoid process of the pterygoid.

499

500   **Septomaxilla (Fig. 8C).** The dome-shaped septomaxilla is located between the vomer and the
501   premaxilla, and rests laterally on the palatal shelf of the maxilla. Dorsally it reaches close to the
502   ventral side of the nasal process of the premaxilla but does not contact this process.

503

504   **Neurocranium**
505   **Parabasisphenoid (Figs. 8B, C, 9B).** The body of the parabasisphenoid is roughly rectangular
506   and bears two long basipterygoid processes that project anterolaterally to meet the pterygoid
507   medially. These processes are flattened near the facet of the pterygoid. Anteriorly, between the
508   basipterygoid processes is a rectangular parasphenoid rostrum. The parabasisphenoid is partly
509   fused to the prootic posterolaterally and to the basioccipital posteriorly.

510

511   **Prootic (Figs. 8C, 9A).** The prootic forms the anterior portion of the otic capsule. It has an
512   anteriorly directed curved and compressed alar process, which approaches the descending
513   process of the parietal and the epipterygoid but does not contact those structures. Below the alar
514   process is the C-shaped incisura prootica, a deep and round notch and exit for the trigeminal
515   nerve. The posterior border of the prootic is marked by the fenestra ovalis, into which the
516   rounded footplate of the stapes inserts. The crista prootica begins at the parabasisphenoid and
517   runs across the lateral side of the prootic. Posterior to its tip and at about the same level as the
518   trigeminal notch is the small foramen for the facial nerve. Dorsally, the prootic contacts the

519   supraoccipital. Ventrally, it articulates with the parabasisphenoid anteromedially and with the
520   basioccipital posteromedially.

521

522   **Otooccipital (Figs. 8A, C, 9B).** The compound otooccipital (fused opisthotic and exoccipital)
523   forms the posterior portion of the otic capsule. It contributes to the composition of the occipital
524   condyle and forms the lateral margin of the foramen magnum. The otooccipital contacts the
525   supraoccipital dorsally and the basioccipital ventrally. Its anterior border contacts the prootic,
526   and has a C-shaped notch, which forms the posterior margin of the fenestra ovalis, and its
527   anterodorsal margin is thickened to form the paroccipital process. Posterolaterally to the fenestra
528   ovalis is the paroccipital process, which contacts the supratemporal and the quadrate laterally.
529   The sphenoccipital tubercle is situated at the junction of the otooccipital and the basioccipital.
530   This tubercle is ventral to the fenestra ovalis, and between both structures is an ellipsoid lateral
531   foramen.

532

533   **Basioccipital (Figs. 8A, 9B).** The pentagonal-shaped basioccipital forms most of the braincase
534   floor. Anteriorly, it is fused to the parabasisphenoid, dorsally it contacts the prootic (anterior) and
535   the otooccipital (posterior). It forms the ventral margin of the occipital condyle.

536

537   **Supraoccipital (Figs. 8A, 9B).** The hourglass-shaped broad supraoccipital forms the roof of
538   both the braincase and otic capsules. The short ascending process of the tectum synoticum
539   originating at the anterior margin of the supraoccipital does not reach the parietal bone. A large
540   posttemporal fenestra is present between the supratemporal and the parietal. The supraoccipital
541   articulates with the dorsal margin of the prootic anterolaterally and with the otooccipital
542   posterolaterally. The posterior border forms the dorsal edge of the foramen magnum.

543

544   **Orbitosphenoid (Fig. 8B, C).** The small paired orbitosphenoids are compressed and L-shaped
545   with the vertex oriented laterally and bearing a small lateral process. The dorsal process is broad
546   and both bones are completely fused medially along this process, forming a slightly bifurcate
547   anterior end of the fused bone. On the ventral surface of the fused dorsal region is a short
548   median, comparatively broad anteroventrally oriented process. The ventral processes of the fused
549   orbitosphenoid bone are slender, directed medially, but distinctly separated. The orbitosphenoid
550   is located anterior to the braincase and posterior and medially with respect to the orbits, at an
551   angle to the dorsoventral axis of the skull.

552

553   **Stapes (Figs. 8B, 9A).** The ossified stapes is composed of a long and slender laterally projecting
554   shaft and a large, rounded footplate, which entire fills the area of the fenestra ovalis. The shaft
555   ends proximal to the posterior crest of the quadrate.

556

557   **Mandible**

558   **Dentary (Figs. 9, 10).** The dentary is the anterior part of the mandible and bears a straight row of
559   22 (right) to 23 (left) teeth loci. Posteriorly, the dentary contacts the coronoid, angular, splenial
560   and surangular. The labial and anteromedial processes of the coronoid clasp the posterodorsal
561   surface of the dentary. Anteriorly, at the lingual surface of the dentary, the opening of Meckel's
562   canal is observed near the mandibular symphysis. The dentary has about five foramina, the
563   anteriormost two are located on the symphyseal region, and the posteriormost is at the level of
564   the midpoint of the dental row.
565
566   **Coronoid (Figs. 9A, 10).** The triradiate coronoid has a long and robust free dorsal coronoid
567   process. The labial process tapers anteriorly up to the level of the gap between the third and
568   fourth posteriormost teeth of the dentary. On the lingual surface of the mandible, the
569   anteromedial process of the coronoid contacts the dentary anteriorly, the splenial ventrally, and
570   the surangular posteriorly. The slender posteromedial process contacts the surangular, but the
571   exact borders are not well resolved in the CT-images. There is a small medial crest between the
572   lower part of the coronoid process and the posteromedial process.
573
574   **Angular (Figs. 9B, 10A, B, D).** The small and slender angular has a pointed anterior and a blunt
575   posterior end. It is located on the ventral surface of the mandible, ventral to the angular process
576   of the dentary. It contacts the surangular posteriorly and the ventral border of the splenial
577   medially. The posterior mylohyoid foramen is visible ventrally at the posterior end where the
578   angular meets the surangular.
579
580   **Splenial (Figs. 9B, 10A, B, D).** The splenial forms the midventral portion of the lingual surface
581   of the mandible. It contacts the dentary anteriorly, the coronoid dorsally, the angular ventrally,
582   and the compound bone posterodorsally. There are two foramina present in the anterior region of
583   the splenial: a larger oval anterior inferior foramen at the suture with the dentary, and a more
584   rounded anterior mylohyoid foramen about half as large, located ventral and posterior to the
585   anterior inferior foramen. The exact borders of the splenial are not well resolved in the CT-
586   images, making it difficult to comment about the exact shape of the bone.
587
588   **Mandibular Compound Bone (Figs. 9, 10).** The compound bone is the posterior part of the
589   mandible and is formed by the fusion of the surangular on the labial surface, and the prearticular
590   and articular on the lingual surface of the mandible. The prearticular forms the floor and the
591   internal margin of the adductor fossa, while the articular forms its posterior margin and provides
592   the articulation to the skull on its dorsal surface. The surangular is located posterior to the
593   dentary and the coronoid and a large surangular foramen is observed next to the contact with the
594   coronoid. Ventral to the surangular is the angular. The retroarticular process is formed by the
595   fused surangular and prearticular-articular complex.
596

597 **Vertebrae (Fig. 15, 16).** There are two sacral vertebrae and 25 presacral vertebrae of which the
598 first three and the last one do not bear ribs.

599

600 **Pectoral Girdle (Fig. 15, 16)**. The pectoral girdle consists of a clavicle, suprascapular,
601 interclavicle, fused scapula and coracoid, epicoracoid, sternum, and xiphisternum. The clavicle is
602 large, triangular, flattened, and encloses a large fenestra. The anterior part of the interclavicle is
603 trifurcate with one median and two anterolaterally oriented processes, each of them about one-
604 fourth the total length of the interclavicle and tapering anteriorly. The median process penetrates
605 anteriorly the posterior third of the suture between the two clavicles. Posteriorly, it has a long,
606 straight, rod-like and posteriorly tapering branch, which surpasses the central part of the sternal
607 fontanelle. The large scapulocoracoid bears a small coracoid fenestra, a large anterior coracoid
608 fenestra, a medium-sized posterior coracoid fenestra, a large scapulocoracoid fenestra, and the
609 glenoid fossa. The rhomboid sternum has a large central fontanelle and is associated with three
610 pairs of sternal ribs. The rod-like xiphisternum has two fenestrae and receives two pairs of
611 xiphisternal ribs. The suprascapula is not visible in ventral view and contacts the scapulocoracoid
612 and the clavicle laterally. The epicoracoid contacts the median edge of the coracoid, but most of
613 this structure is overlain by the interclavicle.

614

615 **Distribution and Natural History (Figs. 16, 17).** *Echinosaura fischerorum* sp. nov. is known
616 from the western slopes of the Andes in northwestern Ecuador, Imbabura and Carchi Provinces,
617 between 1,495–1,750 m (Fig. 17). All known specimen records lie in the lower montane forest
618 ecosystem of the Mira river basin within the Dracula Reserve, a 1,136 ha private protected area
619 managed by the Ecominga foundation. The record from Imbabura province corresponds to a
620 photograph by Jaime Culebras from Manduriacu Reserve of Fundación Ecominga. Most known
621 localities of *E. fischerorum* sp. nov. are in close proximity to the Ecuador-Colombia border and
622 we expect that this species might also be present in neighboring Colombia. Most specimens were
623 observed active among tree roots during the day and collected in pitfall traps along forest ridges
624 near streams. Gravid females were collected in April and November. One female paratype
625 (DHMECN 15210) contained two large oval eggs in the oviduct and several snail shells in the
626 stomach (Fig. 16).

627

628 **Etymology.** The specific epithet is a patronym in honor of Beat Fischer and Urs Fischer, donors
629 who have contributed significantly to the consolidation of the Dracula Reserve in the sectors of
630 Peñas Blancas and El Pailón, which not only protect the populations of this new endemic
631 species, but also important populations of threatened amphibians and reptiles of the Mira river
632 basin.

633

634 **Discussion**

635

636   *Vásquez-Restrepo et al. (2020)* presented an extensive review of *Echinosaura* based on
637   molecular phylogeny, external morphology and biogeography. However, no material was
638   available to those authors for review from extreme southwestern Colombia and northwestern
639   Ecuador, that would have offered the possibility of recognizing additional candidate species of
640   *Echinosaura*.
641
642   The new species is genetically distinct from its congeners and is readily distinguishable based on
643   external morphological characters. By contrast, information on internal morphology of
644   *Echinosaura* is very scarce and to date only few studies (*Bell, Evans & Maisano, 2003; Estes, de*
645   *Queiroz & Gauthier, 1988; Evans, 2008; MacLean, 1974*) have been published with exemplary
646   information on cranial morphology of *Echinosaura*. Furthermore, this information is based only
647   on one specimen of *E. panamensis* (CAS 99994) and two specimens of *E. horrida* (MCZ 18858,
648   USNM 163424) (*Bell, Evans & Maisano, 2003; Evans, 2008*). Here, for the first time a detailed
649   description of the cranial morphology of *Echinosaura* is provided based on CT data of a paratype
650   (DHMECN 15210) of the new species herein described. Unlike *E. horrida* and *E. panamensis*,
651   the nasal bones of *E. fischerorum* sp. nov. are not separated and thus the premaxilla does not
652   meet the frontal. The postfrontal is not excluded from the upper temporal fenestra as indicated by
653   *Evans* (*2008*) for *E. horrida*, but rather expands posteriorly to form the anterior border of the
654   fenestra. Although information on skull morphology of *Echinosaura* is scarce, our data show
655   remarkable interspecific variation suggesting that skull morphological characteristics have
656   taxonomic value. Future studies should therefore examine and compare the skulls of other
657   species of *Echinosaura* to obtain a better overall picture of the skull of the genus. In addition, to
658   estimate the degree of intraspecific variation and thus avoid misinterpretation at the species level,
659   several individuals per species should be examined. Due to possible cryptic diversity within
660   widespread linages, it is also advisable to include type material in the analyses, if possible, in
661   order to be able to make reliable statements about the cranial osteology of the individual species.
662
663   The recognition of *Echinosaura fischerorum* sp. nov. improved our understanding of the
664   diversity and evolutionary history of *Echinosaura*. However, we acknowledge that further
665   phylogenetic and phylogeographic analyses of the populations assigned to *Echinosaura*
666   *fischerorum* sp. nov. from the Río Manduriacu Reserve are needed.
667   The new species described in this paper occurs in a particular area of high endemism and
668   biological diversification in extreme northwestern Ecuador. Therefore, we expect its occurrence
669   in the neighboring country of Colombia, a distribution pattern observed in other species of small
670   vertebrates (*Arteaga et al., 2016; Yánez-Muñoz et al., 2018; Brito et al., 2020; Reyes-Puig et al.*
671   *2020*).
672   In terms of conservation, although the type locality of *Echinosaura fischerorum* sp. nov. is part
673   of the ecological reserves managed by the Ecomiga Foundation, the entire area is threatened by
674   human impacts such as mining concessions and land use changes for logging. The IUCN

675 conservation status of this new species should be evaluated as soon as possible in further studies,
676 as it is very likely to be threatened.
677
Conclusions
678
679
680 Fieldwork in the western foothills of the Andes in northwestern Ecuador led us to the discovery
681 of a new species of *Echinosaura* and increased the number of known species of this genus to
682 eight.
683 Our phylogenetic analyses support the monophyly of *Echinosaura fischerorum* sp. nov. While its
684 sister species *E. horrida* is relatively widespread in the tropical lowland rainforest of western
685 Ecuador, the record of *E. fischerorum* sp nov. from Manduriacu suggests that this species is most
686 likely widespread between Manduriacu Reserve and Río Mira.
687
688

Acknowledgements
689
690 We want to express our gratitude to the Rainforest Trust and their "Species Legacy" program, to
691 Orchid Conservation Alliance, and University of Basel for their support of EcoMinga
692 Foundation's efforts to protect the forest where the new species was discovered. Special thanks to
693 Javier Robayo, Lou Jost, Beat Fischer and Urs Fischer for their continuous support since the
694 beginning of Dracula Reserve. We appreciate the institutional support given by Diego Inclan and
695 Francisco Prieto of INABIO. We thank the collaboration during field work by Callie Broadus,
696 Jaqui Curay, Rocío Manovandas, Rubí García, Jorge Brito, Glenda Pozo, Jordi Salazar, Fausto
697 Recalde, Mateo A. Vega-Yánez, Gabriela Puetate, Pearson McGovern, Natalia Espinoza, Daniel
698 Valencia, Marco Montero, Andy Better, Julio Carrión, Mauricio Herrera-Madrid, Roberto Taicus
699 and the "Dracula´s Rangers" of Ecominga Foundation: Hector Yela, Milton Canticuz, Jeovany
700 Guerra, Rolando Peña, Nilo Ortiz, and David Yela. The work of MYM and JRP is part of the
701 research program Diversidad de Pequeños Vertebrados de Ecuador, supported by INABIO
702 through the project: "Conservación de la Biodiversidad en la Cuenca Binacional de los Ríos
703 Mira-Mataje (MMRB): Construcción de Bases Biofísicas y Socio-ambientales para la
704 Conservación y el Manejo Adaptativo de Servicios Ecosistémicos". Ministerio de Ambiente de
705 Ecuador issued research permits and framework agreement for access to genetic resources. We
706 are grateful to Patrick Campbell (BMNH), Andreas Schmitz (MHNG), Silke Schweiger and
707 Georg Gassner (NMW) for loan of specimens and to Morris Flecks (ZFMK) for taking
708 photographs. Chris Phillips (UIMNH) kindly sent us photographs of the holo- and paratype of *E.
709 keyi*. The "Germany-Brazil-Ecuador Trilateral Cooperation Program" of the GIZ international
710 cooperation provided financial support to MYM and CK. OTC was financially supported by the
711 Deutscher Akademischer Austauschdienst (DAAD). Laboratory work was funded by a grant
712 from SENESCYT (Arca de Noé Initiative; S. R. Ron and O. Torres-Carvajal principal
713 investigators).
714

APPENDIX. Specimens examined.

* Type specimens

Echinosaura fischerorum sp. nov. (n = 9): ECUADOR: Carchi: Reserva Dracula, Sector El Guapilal: DHMECN 15208*, DHMECN 15209*, DHMECN 15210*, DHMECN 15211*; Reserva Dracula, Sector El Pailón Chico: DHMECN 14058*, DHMECN 14059*, DHMECN 14060*, DHMECN 14061*; Reserva Dracula, Cerro Oscuro: DHMECN 12767*.

Echinosaura brachycephala (n = 7): ECUADOR: Cotopaxi: Las Pampas (= San Francisco de las Pampas, -0.418, -78.966, 1,275 m elevation): MHNG 2359.39, ZFMK 46370*, ZFMK 46371*, ZFMK 46372*; Pichincha: Santa Lucía Cloudforest Ecological Reserve (0.0922, -78.620, 1800 m): QCAZ 11913, QCAZ 11918; Santa Lucía Cloudforest Ecological Reserve, Gallo de la Peña trail (0.117, -78.607, 1,932 m): QCAZ 10824.

Echinosaura horrida (n = 6): ECUADOR: ZFMK 7272; Pacific versant of Ecuador: ZFMK 43762, ZFMK 43763, ZFMK 46369; Esmeraldas: Tesoro Escondido Reserve (0.4969600, -79.13682, 620 m): QCAZ 15030; Manabí: Zapote (-0.375, -79.605, 154 m): QCAZ 14506.

Echinosaura keyi (n = 2): ECUADOR: ZFMK 76379; Pichincha: E Rio Baba bridge, 24 km S Santo Domingo de los Colorados, 600 m: UIMNH 80541*.

Echinosaura orcesi (n = 4): ECUADOR: Esmeraldas: road Alto Tambo - El Placer (0.9, -78.616, 585 m): QCAZ 6299; Tesoro Escondido Reserve, Camarón river (0.544, -79.142, 243 m): QCAZ 15026; Carchi: San Marcos, 670 m: NMW 32000:1*; San Marcos, 700 m: NMW 32000:2*.

Echinosaura palmeri (n = 1): COLOMBIA: Chocó: Noananoá, Río San Juan, 30 m: BMNH 1923.10.12.14.

Echinosaura panamensis (n = 7): PANAMA: Coclé: 5-6 km N El Copé: ZFMK 45779, ZFMK 50084, ZFMK 50085, ZFMK 50462, ZFMK 50464, ZFMK 52200, ZFMK 54631.

References

Arteaga A, Pyron RA, Peñafiel N, Romero-Barreto P, Culebras J, Bustamante L, Yánez-Muñoz M, Guayasamin JM. 2016. Comparative phylogeography reveals cryptic diversity and re-peated patterns of cladogenesis for amphibians and reptiles in Northwestern Ecuador. *PloS One* 11(4):e0151746. https://doi.org/10.1371/journal.pone.0151746

747   Beaupre SJ, Jacobson ER, Lillywhite HB, Zamudio K. 2004. *Guidelines for use of live*
748   *amphibians and reptiles in field and laboratory research*. Lawrence, Kansas: American
749   Society of Ichthyologists and Herpetologists.
750   Bell CJ, Evans S, Maisano JA. 2003. The skull of the gymnophthalmid lizard *Neusticurus*
751   *ecpleopus* (Reptilia: Squamata). *Zoological Journal of the Linnean Society*
752   139(2):283–304. https://doi.org/10.1046/j.1096-3642.2003.00077.x
753   Brito J, Koch C, Percequillo AR, Tinoco N, Weksler M, Pinto CM, Pardiñas UF. 2020. A new
754   genus of oryzomyine rodent (Cricetidae, Sigmodontinae) with three new species from
755   montane cloud forests, western Andean cordillera of Colombia and Ecuador. *PeerJ*
756   8:e10247. https://doi.org/10.7717/peerj.10247
757   Castoe TA, Doan TM, Parkinson CL. 2004. Data partitions and complex models in Bayesian
758   analysis: The phylogeny of gymnophthalmid lizards. *Systematic Biology* 53(3):448–469.
759   https://doi.org/10.1080/10635150490445797
760   de Queiroz K. 2007. Species concepts and species delimitation. *Systematic Biology*
761   56(6):879–886. https://doi.org/10.1080/10635150701701083
762   Deng W, Maust BS, Nickle DC, Learn GH, Liu Y, Heath L, Kosakovsky Pond SL, Mullins JI.
763   2010. DIVEIN: a web server to analyze phylogenies, sequence divergence, diversity, and
764   informative sites. *BioTechniques* 48:405–408. doi 10.2144/000113370
765   Estes R, de Queiroz K, Gauthier J. 1988. Phylogenetic relationships within Squamata. In: Estes
766   R, Pregill G, eds. *Phylogenetic relationships of the lizard families*. Stanford, California:
767   Stanford University Press, 119–128.
768   Evans SE. 2008. The skull of lizards and tuatara. In: Gans C, Gaunt AS, Adler K, eds. *Biology of*
769   *the Reptilia, Vol. 20 Morphology H: the Skull of Lepidosauria*. Ithaca, NY: Society for
770   the Study of Amphibians and Reptiles, 1–347.
771   Fitzgerald LA. 2012. Finding and capturing reptiles. In: McDiarmid RW, Foster MS, Guyer C,
772   Gibbons JW, Chernoff N, eds. *Reptile Biodiversity: Standard Methods for Inventory and*
773   *Monitoring*. Oakland, California: University of California Press, 77–88.
774   Fritts TH, Almendáriz A, Samec S. 2002. A new species of *Echinosaura* (Gymnophthalmidae)
775   from Ecuador and Colombia with comments on other members of the genus and
776   *Teuchocercus keyi*. *Journal of Herpetology* 36(3):349–355. 10.1670/0022-
777   1511(2002)036[0349:ANSOEG]2.0.CO;2
778   Goicoechea N, Frost DR, De la Riva I, Pellegrino KCM, Sites Jr J, Rodrigues MT, Padial JM.
779   2016. Molecular systematics of teioid lizards (Teioidea/Gymnophthalmoidea: Squamata)
780   based on the analysis of 48 loci under tree-alignment and similarity-alignment. *Cladistics*
781   32(6):624–671. https://doi.org/10.1111/cla.12150
782   Guindon S, Dufayard JF, Lefort V, Anisimova M, Hordijk W, Gascuel O. 2010. New algorithms
783   and methods to estimate maximum-likelihood phylogenies: assessing the performance of
784   PhyML 3.0. *Systematic Biology* 59(3):307–321. https://doi.org/10.1093/sysbio/syq010
785   Hernández Morales C, Peloso PLV, Bolívar García W, Daza JD. 2019. Skull Morphology of the
786   Lizard *Ptychoglossus vallensis* (Squamata: Alopoglossidae) With Comments on the
787   Variation Within Gymnophthalmoidea. *The Anatomical Record* 302:1074–1092.
788   https://doi.org/10.1002/ar.24038
789   Jerez A, Tarazona OA. 2009. Appendicular skeleton in *Bachia bicolor* (Squamata:
790   Gymnophthalmidae): osteology, limb reduction and postnatal skeletal ontogeny. *Acta*
791   *Zoologica* 90(1):42–50. https://doi.org/10.1111/j.1463-6395.2008.00331.x

792   Katoh K, Standley DM. 2013. MAFFT multiple sequence alignment software version 7:
793   improvements in performance and usability. *Molecular Biology and*
794   *Evolution* 30(4):772–780. https://doi.org/10.1093/molbev/mst010
795   Köhler G, Böhme W, Schmitz A. 2004. A New Species of *Echinosaura* (Squamata:
796   Gymnophthalmidae) from Ecuador. *Journal of Herpetology* 38(1):52–60.
797   https://doi.org/10.1670/164-02A
798   Lanfear R, Calcott B, Ho SYW, Guindon S. 2012. Partition-Finder: Combined selection of
799   partitioning schemes and substitution models for phylogenetic analyses. *Molecular*
800   *Biology and Evolution* 29(6):1695–1701. https://doi.org/10.1093/molbev/mss020
801   Lanfear R, Frandsen PB, Wright AM, Senfeld T, Calcott B. 2017. PartitionFinder 2: New
802   Methods for Selecting Partitioned Models of Evolution for Molecular and Morphological
803   Phylogenetic Analyses. *Molecular Biology and Evolution* 34(3):772–773.
804   https://doi.org/10.1093/molbev/msw260
805   MacLean WP. 1974. Feeding and locomotor mechanism of teiid lizards: Functional morphology
806   and evolution. *Papéis Avulsos de Zoologia* 27:179–213.
807   Marques-Souza S, Prates I, Fouquet A, Camacho A, Kok PJR, Nunes PMS, Dal Vechio F, Sousa
808   Recoder R, Mejia N, Teixeira Junior V, Barrio-Amorós C, Cassimiro J, Dias Lima J, de
809   Sena MA, Rodrigues MT. 2018. Reconquering the water: Evolution and systematics of
810   South and Central American aquatic lizards (Gymnophthalmidae). *Zoologica Scripta*
811   47(3):255–265. https://doi.org/10.1111/zsc.12273
812   Miller M, Pfeiffer W, Schwartz T. 2010. Creating the CIPRES Science Gateway for 1100
813   inference of large phylogenetic trees. In: *Gateway Computing Environments 1101*
814   *Workshop* (GCE). IEEE, 1–8.
815   Nunes PMS, Fouquet A, Curcio FF, Kok PJR, Rodrigues MT. 2012. Cryptic species in *Iphisa*
816   *elegans* Gray, 1851 (Squamata: Gymnophthalmidae) revealed by hemipenial morphology
817   and molecular data. *Zoological Journal of the Linnean Society* 166:361–376.
818   https://doi.org/10.1111/j.1096-3642.2012.00846.x
819   Pellegrino KCM, Rodrigues MT, Yonenaga-Yassuda Y, Sites JW. 2001. A molecular
820   perspective on the evolution of microteiid lizards (Squamata, Gymnophthalmidae), and a
821   new classification for the family. *Biological Journal of the Linnean Society* 74(3):315–
822   338. https://doi.org/10.1006/bijl.2001.0580
823   Rambaut A, Drummond AJ. 2016. TreeAnnotator version 1.8.3. Inc.
824   Reyes-Puig C, Wake D, Kotharambath R, Streicher J, Koch C, Cisneros-Heredia D, Yánez-
825   Muñoz M, Ron S. 2020. Two extremely rare new species of fossorial salamanders of the
826   genus *Oedipina* (Plethodontidae) from northwestern Ecuador. *PeerJ* 8:e9934
827   https://doi.org/10.7717/peerj.9934
828   Rodrigues MT, Teixeira Jr M, Dal Vechio F, Amaro RC, Nisa C, Guerrero AC, Damesco R,
829   Roscito JG, Nunes PMS, Recorder RC. 2013. Rediscovery of the earless microteiid lizard
830   *Anotosaura collaris* Amaral, 1933 (Squamata: Gymnophthalmidae): a redescription
831   complemented by osteological, hemipenial, molecular, karyological, physiological and
832   ecological data. *Zootaxa* 3731(3):345–370. https://doi.org/10.11646/zootaxa.3731.3.5
833   Ronquist F, Teslenko M, van der Mark P, Ayres DL, Darling A, Höhna S, Larget B, Liu L,
834   Suchard MA, Huelsenbeck JP. 2012. MrBayes 3.2: Efficient Bayesian phylogenetic
835   inference and model choice across a large model space. *Systematic Biology* 61:539–542.
836   https://doi.org/10.1093/sysbio/sys029

837 Roscito JG, Rodrigues MT. 2010. Comparative cranial osteology of fossorial lizards from the
838   tribe gymnophthalmini (Squamata, Gymnophthalmidae). *Journal of Morphology*
839   271(11):1352–1365. https://doi.org/10.1002/jmor.10878
840 Savage JM. 1997. On terminology for the description of the hemipenis of squamate reptiles.
841   *Herpetological Journal* 7:23–25.
842 Stamatakis A. 2014. RAxML Version 8: A tool for phylogenetic analysis and post-analysis of
843   large phylogenies. *Bioinformatics* 30(9):1312–1313.
844   https://doi.org/10.1093/bioinformatics/btu033
845 Stamatakis A, Hoover P, Rougemont J. 2008. A rapid bootstrap algorithm for the RAxML Web
846   servers. *Systematic Biology* 57(5):758–771. https://doi.org/10.1080/10635150802429642
847 Torres-Carvajal O, Lobos SE, Venegas PJ, Chávez G, Aguirre-Peñafiel V, Zurita D, Echeverría
848   L. 2016. Phylogeny and biogeography of the most diverse clade of South American
849   gymnophthalmid lizards (Squamata, Gymnophthalmidae, Cercosaurinae). *Molecular*
850   *Phylogenetics and Evolution* 99:63–75. https://doi.org/10.1016/j.ympev.2016.03.006
851 Torres-Carvajal O, Pazmiño-Otamendi G, Ayala-Varela F, Salazar-Valenzuela D. 2021. Reptiles
852   del Ecuador. Version 2021.1. Museo de Zoología, Pontificia Universidad Católica del
853   Ecuador. Available at *https://bioweb.bio/faunaweb/reptiliaweb* (accessed 02 July 2021).
854 Uzzell T. 1973. A revision of lizards of the genus *Prionodactylus*, with a new genus for *P.*
855   *leucostictus* and notes on the genus *Euspondylus* (Sauria, Teiidae). *Postilla* 159:1–67.
856 Uzzell TM Jr. 1965. Teiid Lizards of the genus *Echinosaura*. *Copeia* 1965(1):82–89.
857   https://doi.org/10.2307/1441244
858 Vásquez-Restrepo JD, Ibáñez R, Sánchez-Pacheco SJ, Daza JM. 2020. Phylogeny, taxonomy
859   and distribution of the Neotropical lizard genus *Echinosaura* (Squamata:
860   Gymnophthalmidae), with the recognition of two new genera in Cercosaurinae.
861   *Zoological Journal of the Linnean Society* 189(1):287–314.
862   https://doi.org/10.1093/zoolinnean/zlz124
863 Yánez-Muñoz M, Reyes-Puig C, Reyes-Puig J, Velasco J, Ayala-Varela F, Torres-Carvajal O.
864   2018. A new cryptic species of *Anolis* lizard from northwestern South America
865   (Iguanidae, Dactyloinae). *ZooKeys* 794:135–163.
866   https://doi.org/10.3897/zookeys.794.26936
867 Yánez-Muñoz MH, Batallas D, Franco-Mena D, Meza-Ramos PA, Oyagata LA, PadillaD,
868   Paucar C, Reyes-Puig JP, Rodríguez A, Urgilés-Merchán MA, Vega-Yánez M. 2020.
869   *Anfibios en los Ecosistemas Andino-Tropicales de la provincia del Carchi*. INABIO –
870   GADPC.
871
872
873

Variation in selected morphological characters of the different species of *Echinosaura.*

n = number of specimens studied; SVL = snout–vent length.

1 **Table 1.** Variation in selected morphological characters of the different species of *Echinosaura*. n = number of specimens studied; SVL = snout–
2 vent length.

SPECIES	*E. fischerorum* sp nov. (n=9)	*E. brachycephala* (n=25)	*E. centralis* (n=39)	*E. horrida* (n=27)	*E. keyi* (n=14)	*E. orcesi* (n=4)	*E. palmeri* (n=44)	*E. panamensis* (n=10)
Max. SVL males (mm)	69 (n=3)	72 (n=10)	75	86 (n=14)	80 (n=7)	70 (n=2)	80	71 (n=5)
Max. SVL females (mm)	67 (n=9)	78 (n=15)	77	80 (n=13)	64 (n=7)	81 (n=2)	74	74 (n=5)
Internasal	Single	Single	Divided	Single	Divided	Single	Divided	Divided
Frontal	Single	Single	Single	Single	Single (rarely divided)	Single	Single	Divided
Subcaudals per caudal segment	3	4	3	3	3	5-6	3	3
Supralabials	5–5	3–5	4–6	4–6	4–5	3–5	4–5	4–6
Infralabials	4–4	3	3–5	3–4	3–5	2–3	4–5	4–6
Femoral pores	7–9	7–9	4–9	7–10	8–11	5–15	6–10	3–9
Subdigital lamellae on 4th finger	14–18	14–23	12–18	14–19	17 (n=1)	20–22	12–17	13–16
Subdigital lamellae on 4th toe	23–27	23–32	20–27	21–25	28 (n=1)	30–36	19–25	20–22
Temporal and nuchal scales	A pair of sharp spine like scales in temporal and nuchal region	Low rounded tubercles surrounded by granular scales	Temporal region tuberculated, and nuchal region with two rows of enlarged	Low tubercles in temporal region and subconical tubercles in nuchal region	Flat temporal scales and low enlarged tubercles in nuchal region	Flat temporal scales and low tubercles surrounded by granular scales in nuchal region	Flat temporal scales and enlarged, slightly keeled nuchal tubercles surrounded by	Flat temporal scales and enlarged, slightly keeled nuchal tubercles surrounded by

			subconical tubercles on each side of the body				granular scales	small rounded scales
Scales of dorsum	Vertebral row of paired, enlarged, keeled scales and two paravertebral series of short oblique rows of projecting scales	Two paravertebral rows of tubercles or spine-like scales, separated by 4-6 small scales	Two paravertebral rows of spine-like scales, separated by 5 or mores irregular scales	Vertebral row of paired, enlarged, smooth scales	Paravertebral rows formed by spine-like scales, discontinuous posteriorly	No continuous vertebral or paravertebral rows of enlarged scales: enlarged scales arranged obliquely in short series of 3–8 scales forming irregular chevrons on dorsal field of body and broken undulating rows of scales along dorsolateral body	Two paravertebral rows separated by 3-8 small irregular scales	Two paravertebral rows of tubercular scales arranged in zigzag pattern
Scales of flanks	Enlarged spiny scales forming oblique lines	Tubercular scales forming oblique lines on lateral surface of body	Series of spine-like scales forming oblique lines on lateral surface of body	Series of spine-like scales forming oblique lines on lateral surface of body	Series of conical scales of different sizes forming oblique lines on lateral surface of body	Alternate tubercular scales on lateral surface of body	Series of spine-like scales forming oblique lines on lateral surface of body	Series of tubercular scales forming oblique lines on lateral surface of body
Source	This study	Köhler et al. 2004	Vásquez-Restrepo et al. 2019	Uzzell 1965; Köhler et al. 2004; This study	Köhler et al. 2004; Vásquez-Restrepo et al. 2019; This study	Fritts et al. 2002	Vásquez-Restrepo et al. 2019	Vásquez-Restrepo et al. 2019

Morphometric data of the type series of *Echinosaura fischerorum* sp. nov.

Holotype is marked with *. Accompanying the range, the sample size is included in parentheses (N), followed by the mean and standard deviation. All specimens are from the same collection (DHMECN). SVL = snout–vent length; TRL = trunk length; TAL = tail length; SL = snout length; HL = head length; HW = head width; HUM = humerus length; FAL = forearm length; HND = hand length; FEM = femur length; TIB = tibia length; FTL = foot length.

1 **Table 2.** Morphometric data of the type series of *Echinosaura fischerorum* sp. nov. Holotype is marked with *. Accompanying the range, the
2 sample size is included in parentheses (N), followed by the mean and standard deviation. All specimens are from the same collection (DHMECN).
3 SVL = snout–vent length; TRL = trunk length; TAL = tail length; SL = snout length; HL = head length; HW = head width; HUM =
4 humerus length; FAL = forearm length; HND = hand length; FEM = femur length; TIB = tibia length; FTL = foot length.

	Males				Range	Females				Range	Juveniles			Range
Character	**15208***	**15209**	**15211**	**16110**		**14058**	**14060**	**15210**	**16109**		**14059**	**14061**	**12767**	
SVL	69	62.8	54.7	63.1	69–54.7 (4) 66.05 ± 4.17	66.8	63.8	65.2	61.4	66.8–61.4 (4) 64.1 ± 3.81	29.6	52.7	40.5	52.7–29.6 (3) 40.93 ± 11.56
TRL	33.6	27.2	28.2	28.1	33.6–22.7 (4) 30.04 ± 4.52	25.5	26.1	29.5	27.6	29.5–25.5 (4) 27.5 ± 2.82	13.1	19.6	15.9	19.6–13.1 (3) 16.2 ± 3.26
TAL	89.5	85.2	67	88.2	89.5–67 (4) 78.25 ± 15.91	82.5	84	88.7	91	91–82.5 (4) 86.75 ± 6.01	37.5	73.6	55.6	73.6–37.5 (3) 55.57 ± 18.05
SL	13.7	11.8	10.8	12	13.7–10.8 (4) 12.25 ± 2.05	12.1	12.2	12.6	12	12.6–12 (4) 12.3 ± 0.42	5.7	9.4	7.3	9.4–5.7 (3) 7.47 ± 1.86
HL	20.1	17.5	17.6	18.3	20.1–17.5 (4) 18.8 ± 1.83	18.5	17.2	17.2	16.3	18.5–16.3 (4) 17.4 ± 1,55	8.8	15.2	11	15.2–8.8 (3) 11.67 ± 3.25
HW	13.2	12.1	10.7	11.9	13.2–10.7 (4) 11.95 ± 1.76	11.6	10.7	10.6	11	11.6–10.6 (4) 11.1 ± 0.70	5.2	9.5	7.1	9.5–5.2 (3) 7.27 ± 2.15
HUM	9.7	7.9	8.4	7.9	9.7–7.9 (4) 8.8 ± 1.27	10.9	9.3	8.4	9	10.9–8.4 (4) 9.65 ± 1.76	4.6	7.7	6.4	7.7–4.6 (3) 6.23 ± 1.56
FAL	9.1	7.4	7.3	8.3	9.1–7.3 (4) 8.2 ± 1.27	8	7.7	7.1	8.1	8.1–7.1 (4) 7.6 ± 0.70	3.9	6.1	4.7	6.1–3.9 (3) 4.9 ± 1.11
HND	9.3	8.4	9	8.6	9.3–8.4 (4) 8.85 ± 0.63	9.7	14.8	8.2	9.9	14.8–8.2 (4) 11.5 ± 4.66	4.4	8.4	5.8	8.4–4.4 (3) 6.2 ± 2.03
FEM	12.5	11	10.7	13.1	13.1–10.7 (4) 11.9 ± 1.69	11.6	12.1	9.6	11.2	12.1–9.6 (4) 10.85 ± 1.76	5.5	9.6	6.3	9.6–5.5 (3) 7.13 ± 2.17
TIB	13.7	11.4	10.9	11.3	13.7–10.9 (4) 12.3 ± 1.98	10.7	10.6	9.9	10.8	10.8–9–9 (4) 10.35 ± 0.63	5.3	9.8	5.8	9.8–5.3 (3) 6.97 ± 2.47
FTL	15.7	14.7	14.9	14.2	15.7–14.2 (4) 14.95 ± 1.06	15.2	14.9	15.5	15.4	15.5–14.9 (4) 15.2 ± 0.42	7.3	13.8	8	13.8–7.3 (3) 9.70 ± 3.57

Lepidotic characters of the type series of *Echinosaura fischerorum* sp. nov.

1   **Table 3.** Lepidotic characters of the type series of *Echinosaura fischerorum* sp. nov.

Character	Males	Females	Juveniles
Frontal scales	1	1	1
Large chin shields	2	2	2
Gulars in transverse row	19–20	17–21	18–19
Internasal scales	1	1	1
Frontonasal scales	2	2	2
Frontoparietal scales	2	2	2
Supraoculars	3	3	3
Presupraoculars	1	1	1
Postmentals	1	1	1
Mentals	1	1	1
Scales between paravertebral edges	10–11	10–11	9–10
Supralabial scales	5–5	5–5	5–5
Infralabial scales	4–4	4–4	4–4
Femoral pores	8–9	0	7–8
Lamellae under the fourth finger: left, right	16–18/14–18	16–18/15–17	15–18/14–17
Lamellae under the fourth toe: left, right	24–26	24–27/24–26	24–25/23–26
Subcaudal scales per autotomic segment	3	3	3

Figure 1

Phylogeny of Cercosaurinae, with a close-up of *Echinosaura*.

Maximum clade credibility tree obtained from a Bayesian analysis of 148 taxa and 1,935 characters. Numbers above branches are Bayesian posterior probability (PP) values and those below branches are ML bootstrap support (BS) values.
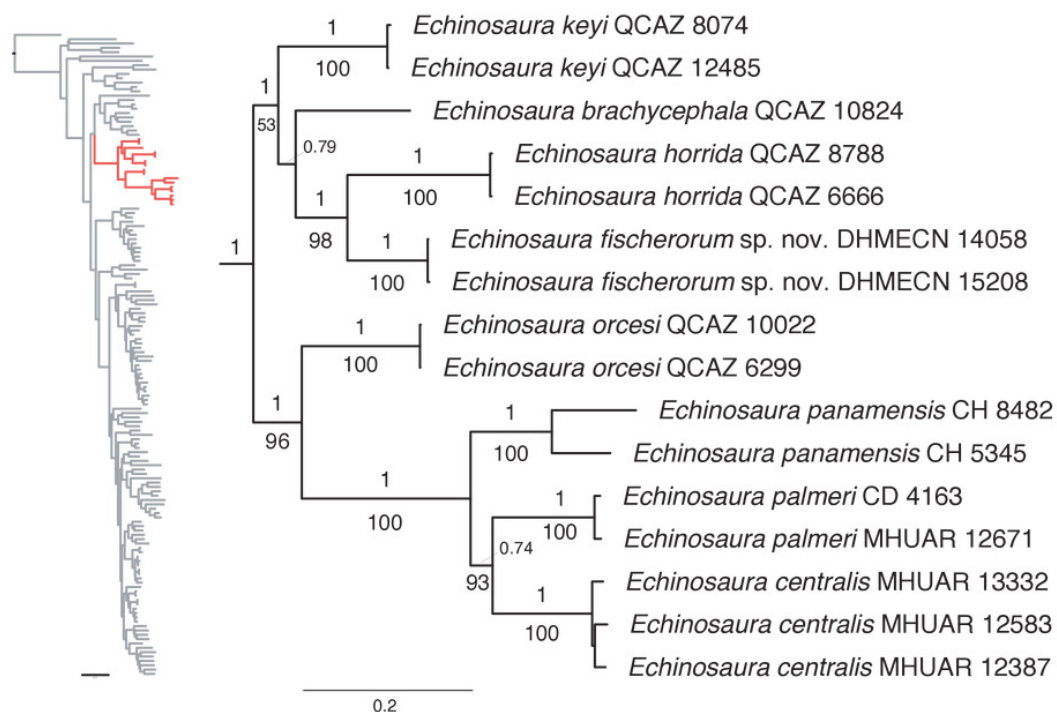
Figure 2

Holotype of *Echinosaura fischerorum* sp. nov. (male, DHMECN 15208) in dorsal (upper left), ventral (upper right), and lateral (bottom) views.

Scale bars = 10 mm. Photographs by MYM.

Figure 3

Head of the holotype of *Echinosaura fischerorum* sp. nov. (male, DHMECN 15208).

(A) dorsal view, (B) lateral view and (C) ventral view. Scale bar = 10 mm. Infralabial and mental scales are shown in gray in ventral view. Illustrations by MYM.
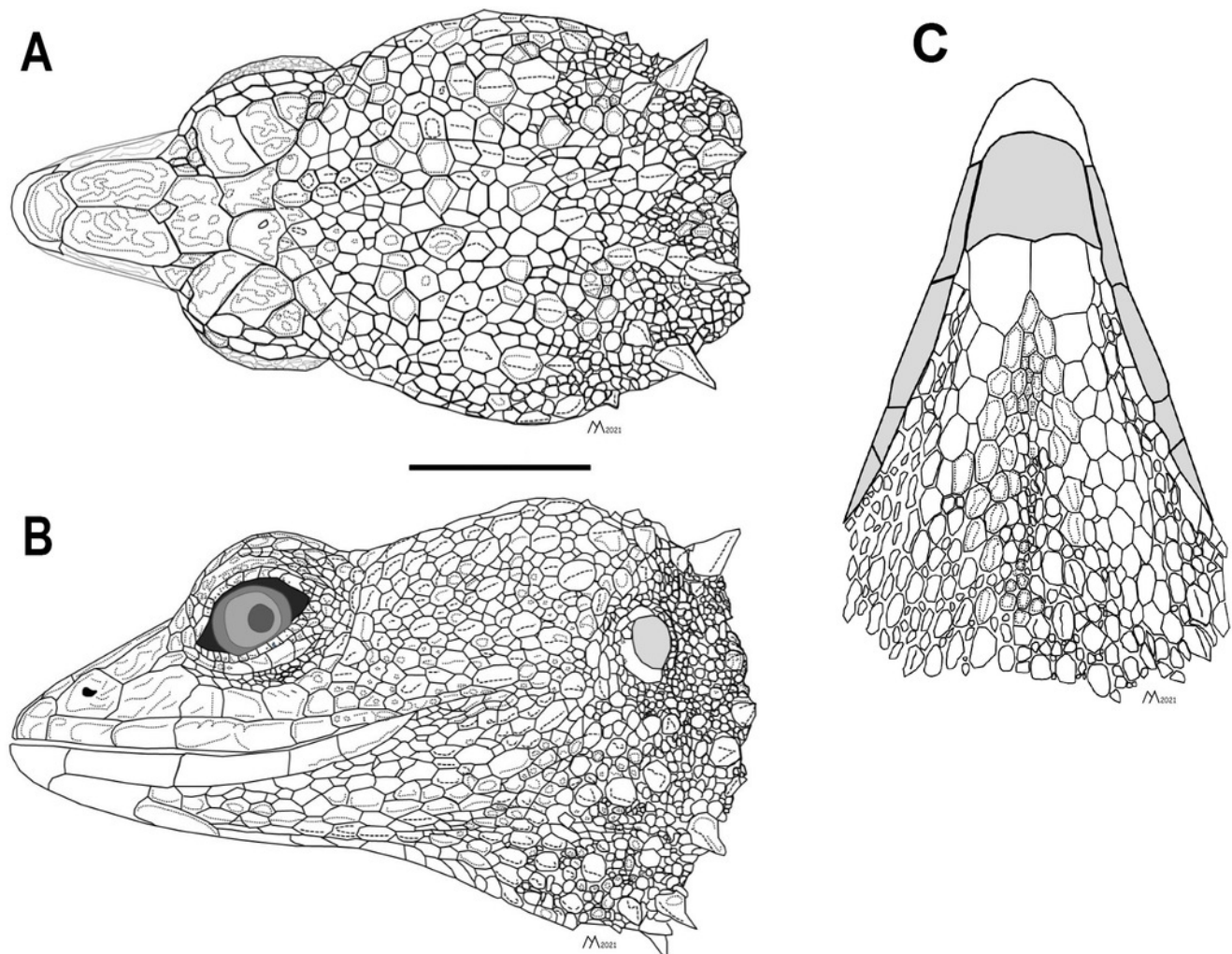
Figure 4

Preserved type specimens of *Echinosaura fischerorum* sp. nov. showing color variation in dorsal view.

Top (males): DHMECN 15208 (Holotype), DHMECN 15209 (Paratype), DHMECN 15211 (Paratype); middle (females): DHMECN 15210 (Paratype), DHMECN 14058 (Paratype), DHMECN 14060 (Paratype); bottom (juveniles): DHMECN 14061 (Paratype), DHMECN 12767 (Paratype), DHMECN 14059 (Paratype). Scale bars = 10 mm. Photographs by MYM.

Figure 5

Preserved type specimens of *Echinosaura fischerorum* sp. nov. showing color variation in ventral view.

Top (males): DHMECN 15208 (Holotype), DHMECN 15209 (Paratype), DHMECN 15211 (Paratype); middle (females): DHMECN 15210 (Paratype), DHMECN 14058 (Paratype), DHMECN 14060 (Paratype); bottom (juveniles): DHMECN 14061 (Paratype), DHMECN 12767 (Paratype), DHMECN 14059 (Paratype). Photographs by MYM.

Figure 6

Live type specimens of *Echinosaura fischerorum* sp. nov. showing color variation in dorsal view.

(A) DHMECN 15208, male (Holotype); (B) DHMECN 15209, male; (C) DHMECN 15211, male; (D) DHMECN 16109, female; (E) DHMECN 16110, male. Scale bars = 10 mm. Photographs by JPRP (A, B, C); MAUM (D); Andrew Better (E).
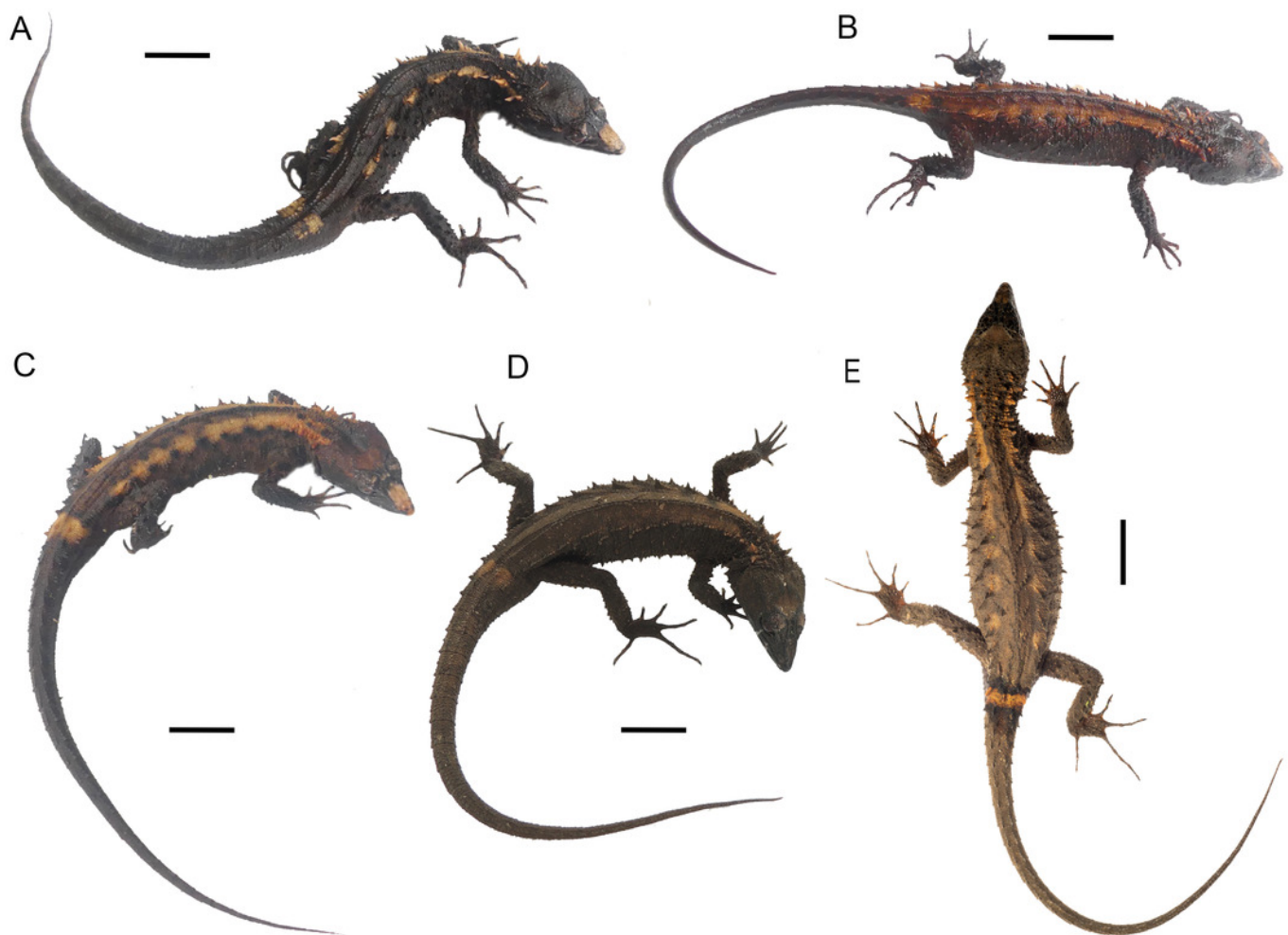
Figure 7

Right hemipenis of male holotype of *Echinosaura fischerorum* sp. nov. (DHMECN 15208, Holotype) in (A) asulcate, (B) lateral, (C) sulcate, and (D) apical views.

Scale bar = 10 mm. Photographs by Morris Flecks.
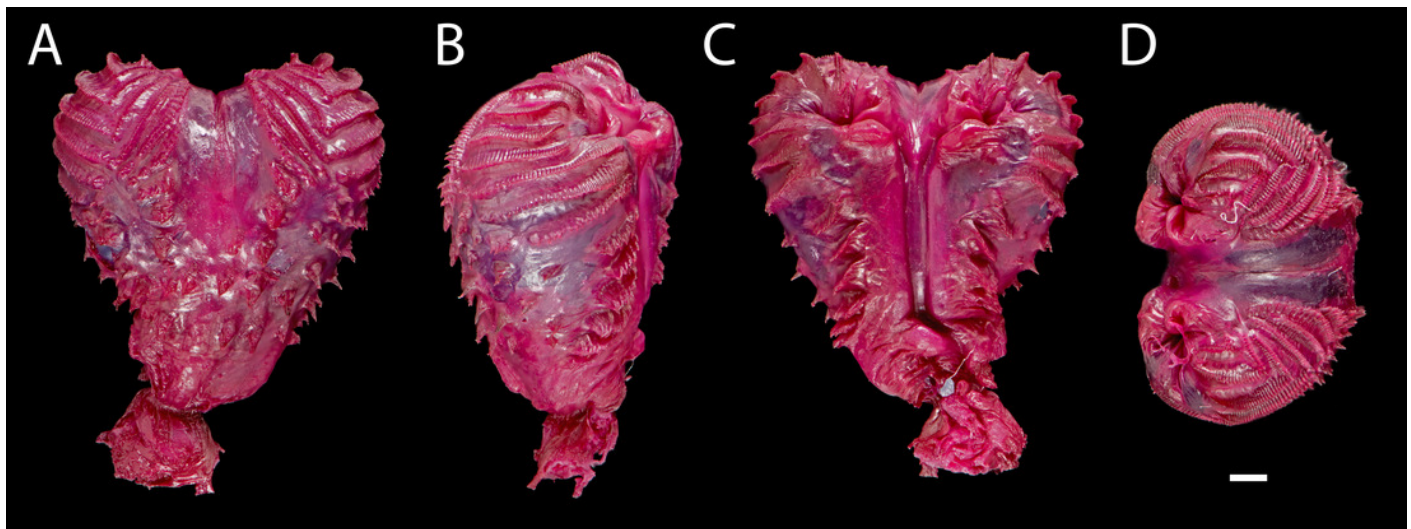
Figure 8

Cranial skeleton of female paratype (DHMECN 15210) of *Echinosaura fischerorum* sp. nov.

The skull is shown without mandible in (A) dorsal, (B) ventral, (C) lateral views. Bo = basioccipital; Ec = ectopterygoid; Ep = epipterygoid; F = frontal; J = jugal; Mx = maxilla; N = nasal; Os = orbitosphenoid; Ot = otoccipital; P = parietal; Pa = palatine; Pfr = postfrontal; Po = postorbital; Pr = prootic; Prf = prefrontal; Ps = parabasisphenoid; Pt = pterygoid; Px = premaxilla; Q = quadrate; Sc = scleral ossicles; Sm = septomaxilla; So = supraoccipital; Sq = squamosal; St = supratemporal; Stp = stapes; Vo = vomers. Scale bars = 1 mm.
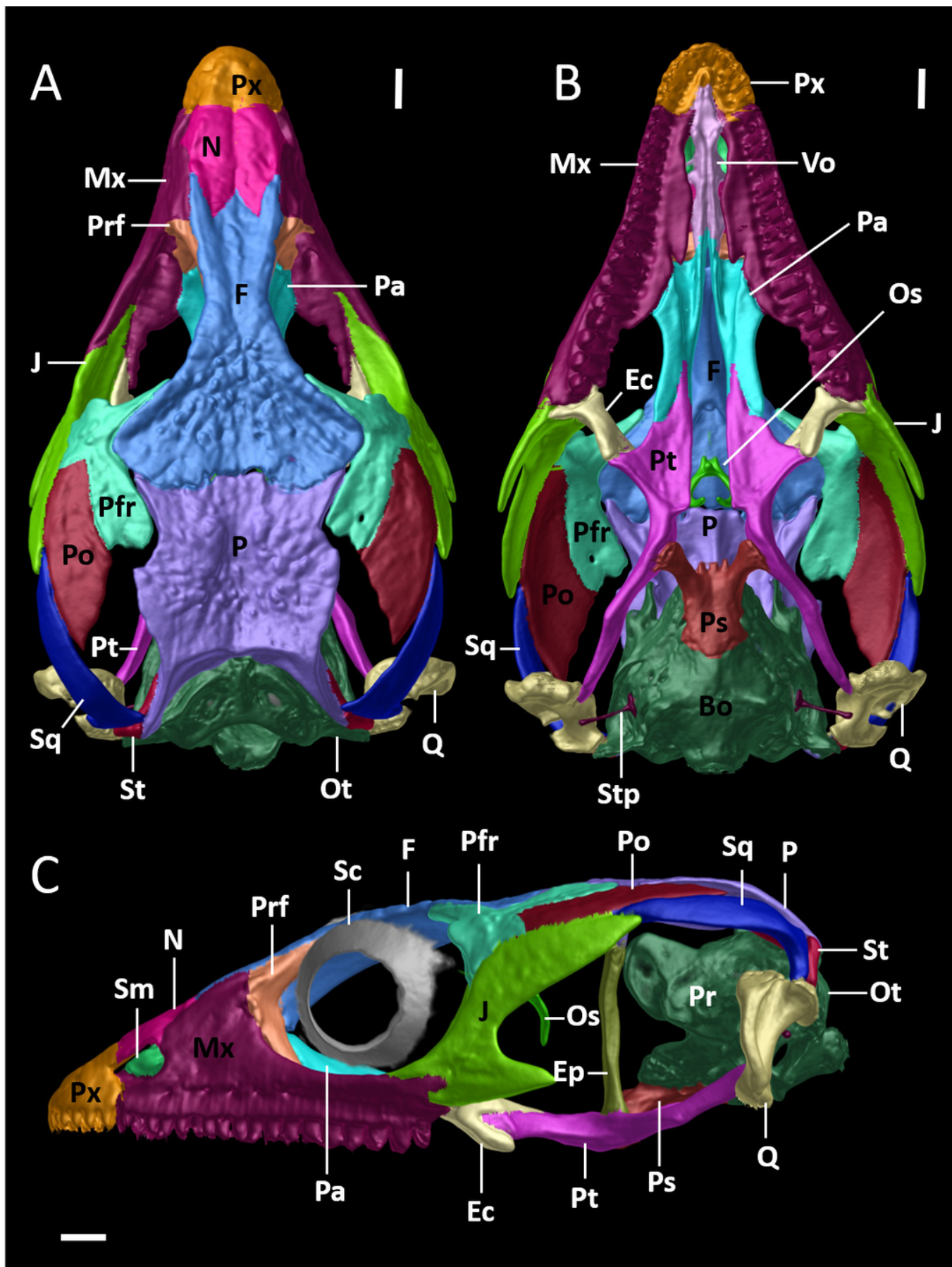
Figure 9

Cranial skeleton of female paratype (DHMECN 15210) of *Echinosaura fischerorum* sp. nov.

The skull is shown in (A) anterior and (B) posterior views. An = angular; Bo = basioccipital; Co = coronoid; D = dentary; Ep = epipterygoid; F = frontal; J = jugal; Mx = maxilla; N = nasal; Ot = otoccipital; P = parietal; Pfr = postfrontal; Po = postorbital; Pr = prootic; Ps = parabasisphenoid; Pt = pterygoid; Px = premaxilla; Rp = retroarticular process; Q = quadrate; San = surangular; Sp = splenial; Sq = squamosal; St = supratemporal; Stp = stapes. Scale bar = 1 mm.
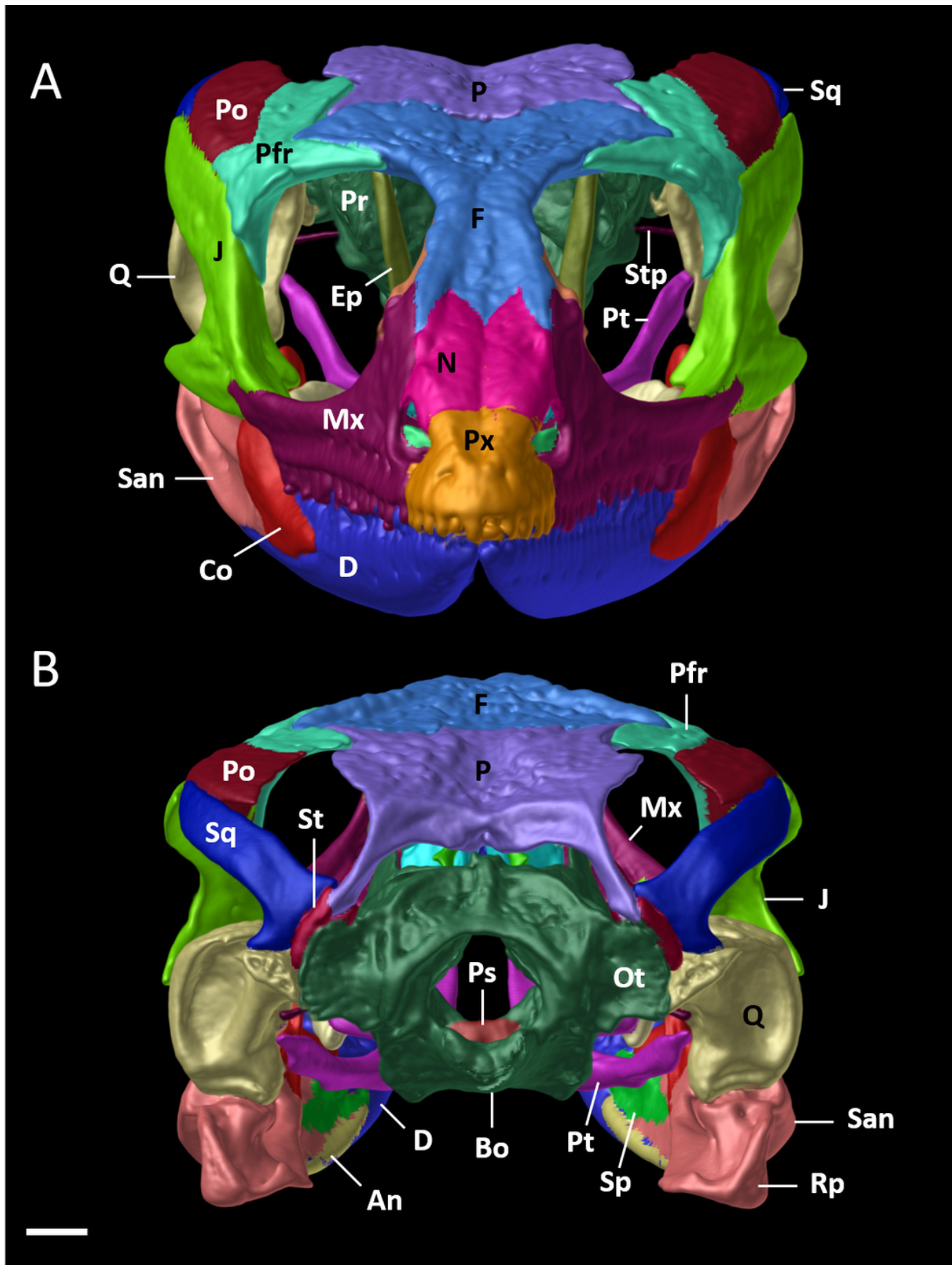
Figure 10

Mandible of female paratype (DHMECN 15210) of *Echinosaura fischerorum* sp. nov. in
(A) dorsal, (B) ventral, (C) lateral, and (D) medial views.

An = angular; Co = coronoid; D = dentary; Rp = retroarticular process; San = surangular; Sp
= splenial. Scale bar = 1 mm.
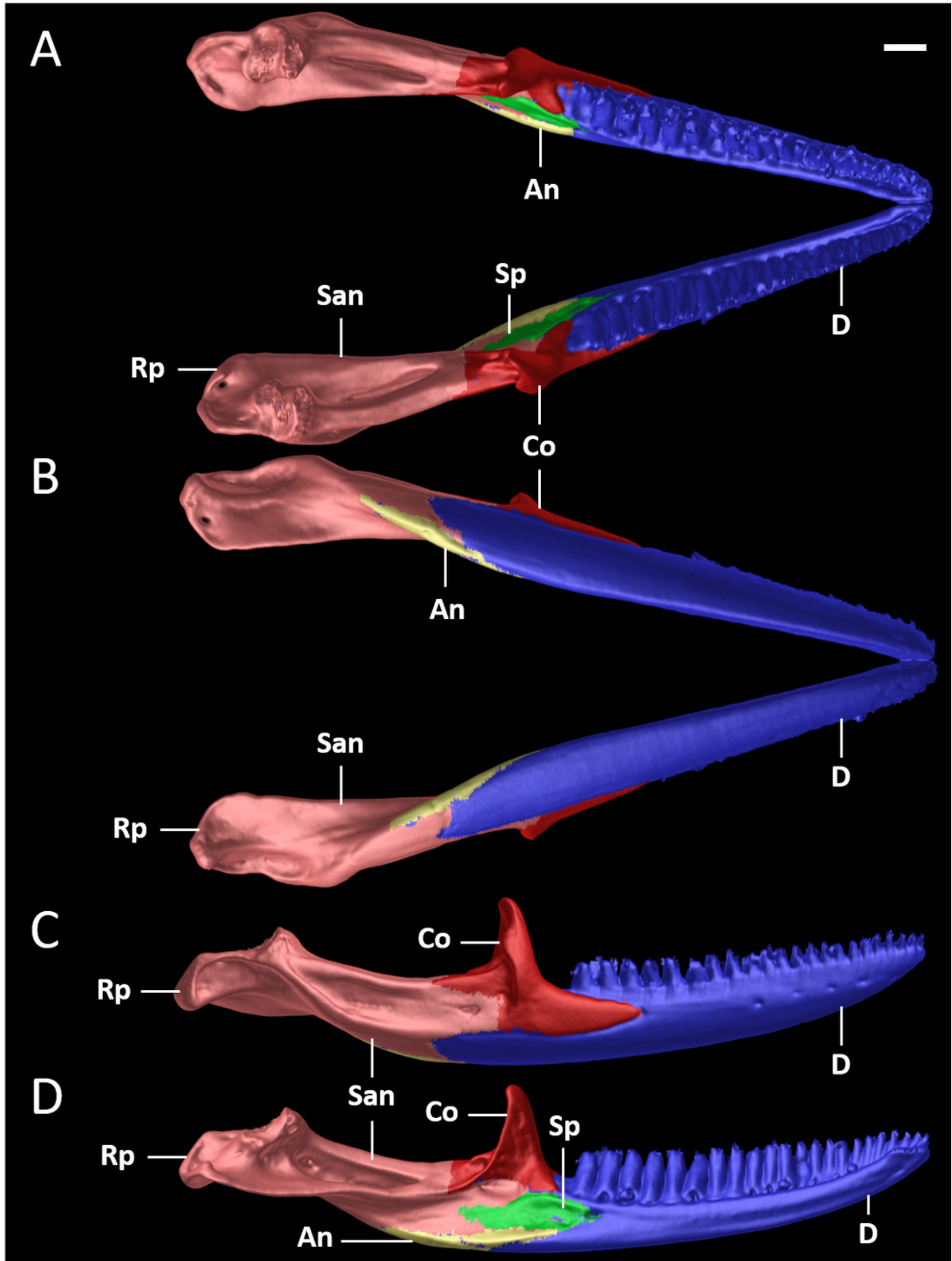
Figure 11

Heads of seven species of *Echinosaura* in dorsal (left) and lateral (right) views.

(A) *Echinosaura fischerorum* sp. nov. (DHMECN 15208, Holotype), (B) *E. horrida* (ZFMK 43763), (C) *E. brachycephala* (ZFMK 46370, Paratype), (D) *E. keyi* (UIMNH 80451, Holotype), (E) *E. palmeri* (BMNH 1923.10.12.14), (F) *E. panamensis* (ZFMK 52200), (G) *E. orcesi* (NMW 32000:1, Paratype). Scale bar = 5 mm. Photographs by MYM (A); Morris Flecks (B, C, E–G); Chris Phillips (D).
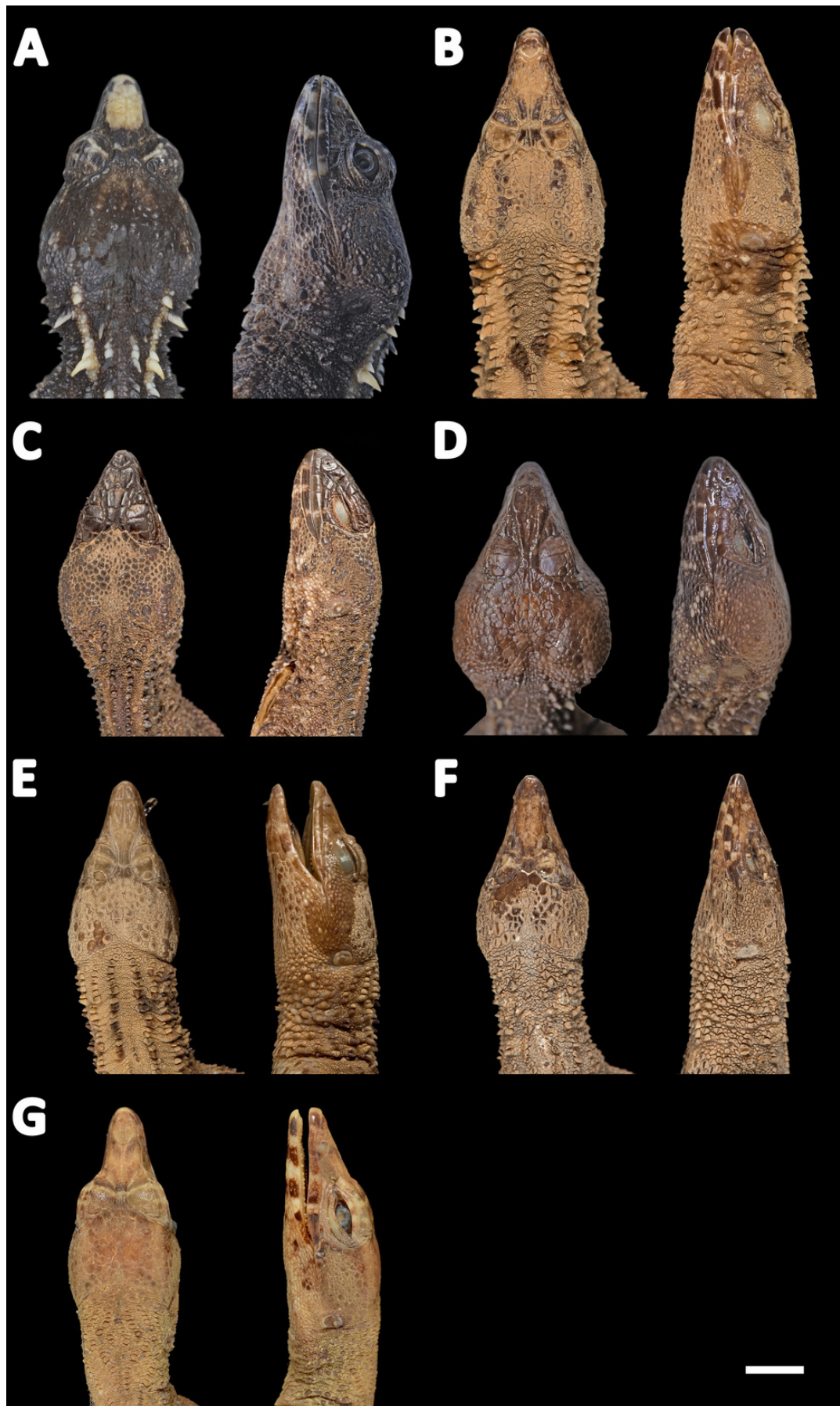
Figure 12

Midbody of seven species of *Echinosaura* in dorsal view.

(A) *Echinosaura fischerorum* sp. nov. (DHMECN 15209, Paratype), (B) *E. horrida* (ZFMK 43763), (C) *E. brachycephala* (ZFMK 46370, Paratype), (D) *E. keyi* (UIMNH 80451, Holotype), (E) *E. palmeri* (BMNH 1923.10.12.14), (F) *E. panamensis* (ZFMK 52200), (G) *E. orcesi* (NMW 32000:2, Paratype). Scale bar = 5 mm. Photographs by MYM (A); Morris Flecks (B, C, E–G); Chris Phillips (D).

Figure 13

Tails of seven species of *Echinosaura* in dorsal (left) and ventral (right) views.

(A) *Echinosaura fischerorum* sp. nov. (DHMECN 15208, Holotype), (B) *E. horrida* (ZFMK 43763), (C) *E. brachycephala* (ZFMK 46370, Paratype), (D) *E. keyi* (UIMNH 80451, Holotype), (E) *E. palmeri* (BMNH 1923.10.12.14), (F) *E. panamensis* (ZFMK 52200), (G) *E. orcesi* (NMW 32000:2, Paratype). Scale bar = 5 mm. Photographs by MYM (A); Morris Flecks (B, C, E–G); Chris Phillips (D).
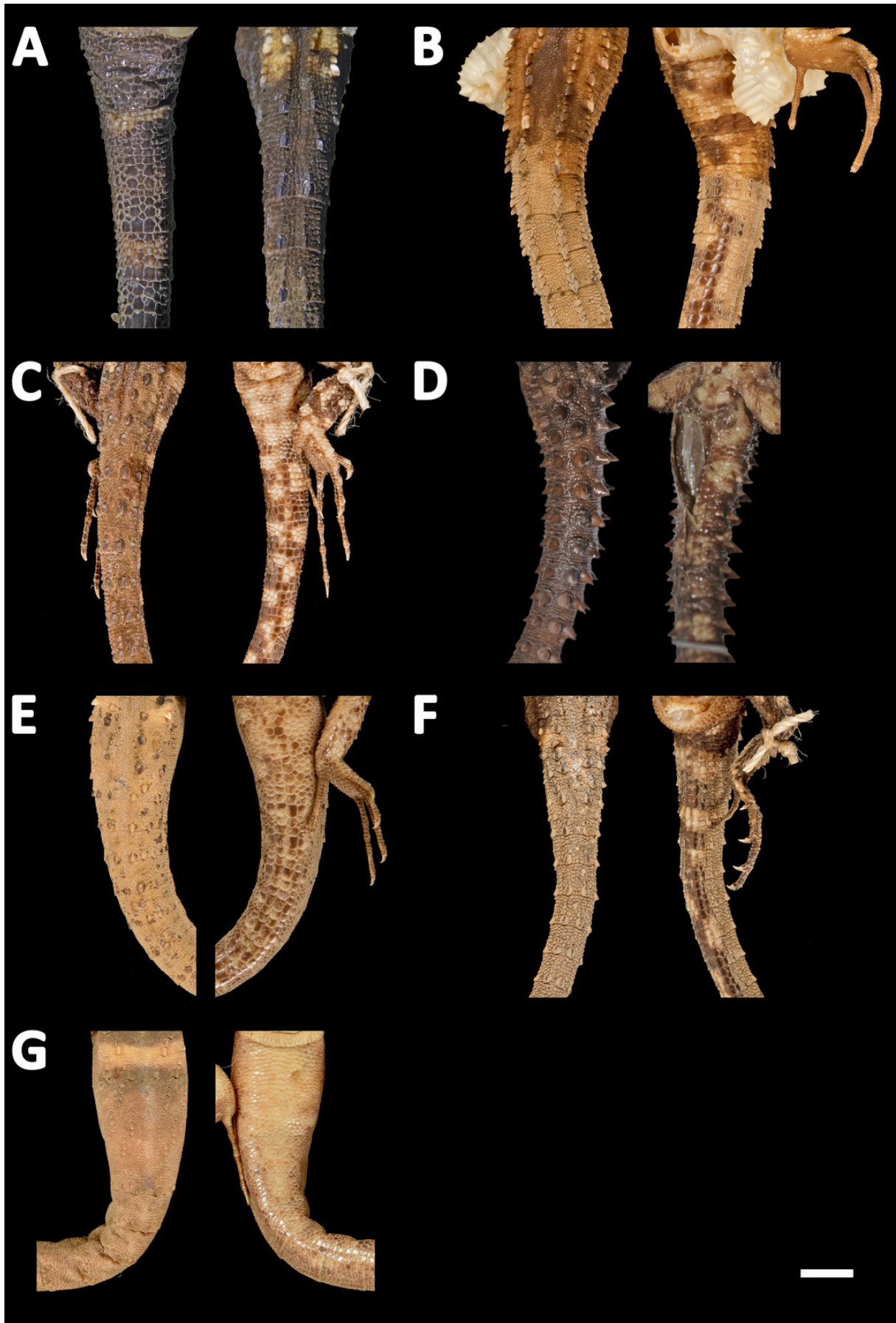
Figure 14

Live specimens of six species of *Echinosaura*.

(A) *E. fischerorum* sp. nov., male (no voucher), Reserva Manduriacu, Pichincha, Ecuador; (B) *E. horrida,* male (DHMECN 13913), Cerro Zapallo, Esmeraldas, Ecuador; (C) *E. palmeri,* male (no voucher), Timbiqui, Colombia; (D) *E. brachycephala,* male (QCAZ 11911), Reserva Ecológica Bosque Nublado Santa Lucía, Pichincha, Ecuador; (E) *E. keyi,* male (QCAZ 8074), Reserva Otokiki, Esmeraldas, Ecuador; (F) *E. orcesi,* male (QCAZ 15026), Reserva Tesoro Escondido, Esmeraldas, Ecuador. Photographs by MYM (B); Jaime Culebras (A, C); Diego Quirola (D, E); Santiago R. Ron (F).
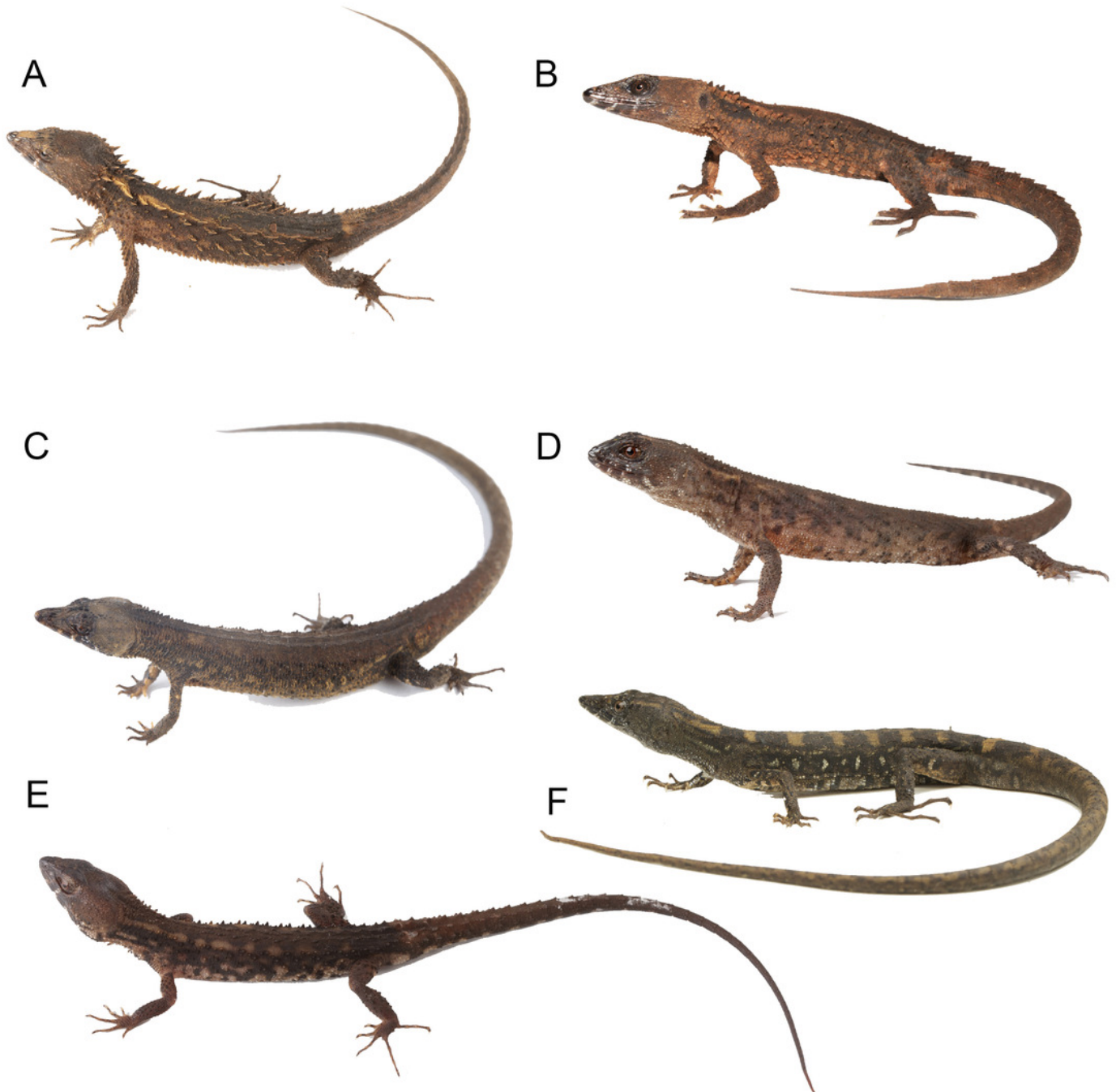
Figure 15

Pectoral girdles of female paratype DHMECN 15210 (A, B) and male holotype DHMECN 15208 (C, D) of *Echinosaura fischerorum* sp. nov. in ventral (left) and dorsal (right) views.

Acf = anterior coracoid fenestra; Cf = coracoid fenestra; Cl = clavicle; Ep = epicoracoid; Gf = glenoid fossa; In = interclavicle; Pcf = posterior coracoid fenestra; R = ribs; Sc = scapulocoracoid; Scf = scapula-coracoid fenestra; Sf = sternal fenestra; Sp = suprascapula; St = Sternum; Xs = xiphisternum. Scale bars = 5 mm.
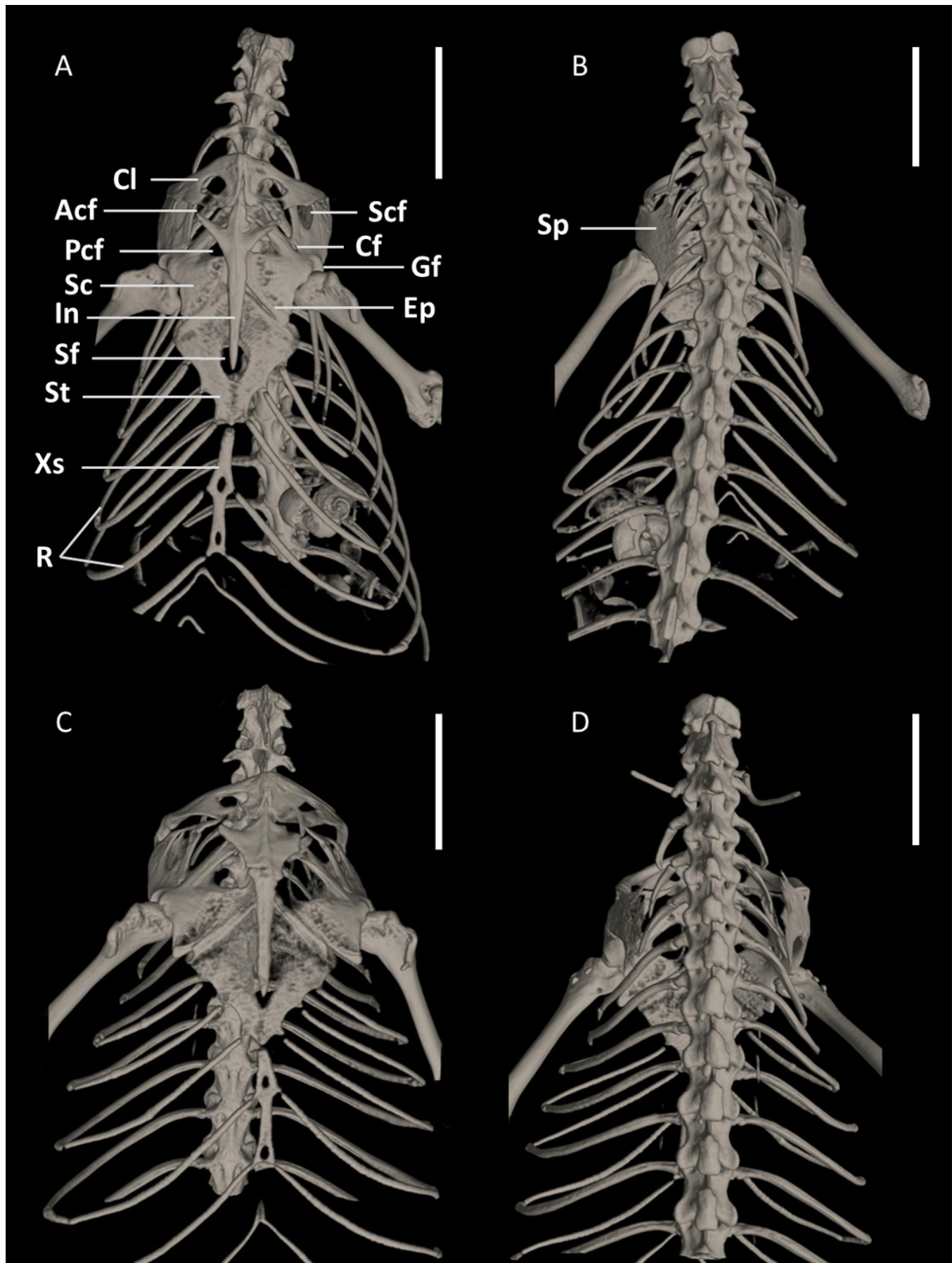
Figure 16

X-ray images of *Echinosaura fischerorum* sp. nov. (A) Male holotype (DHMECN 15208); (B) female paratype (DHMECN 15210).

Red arrows show snail shells in the stomach; green arrows show eggs.
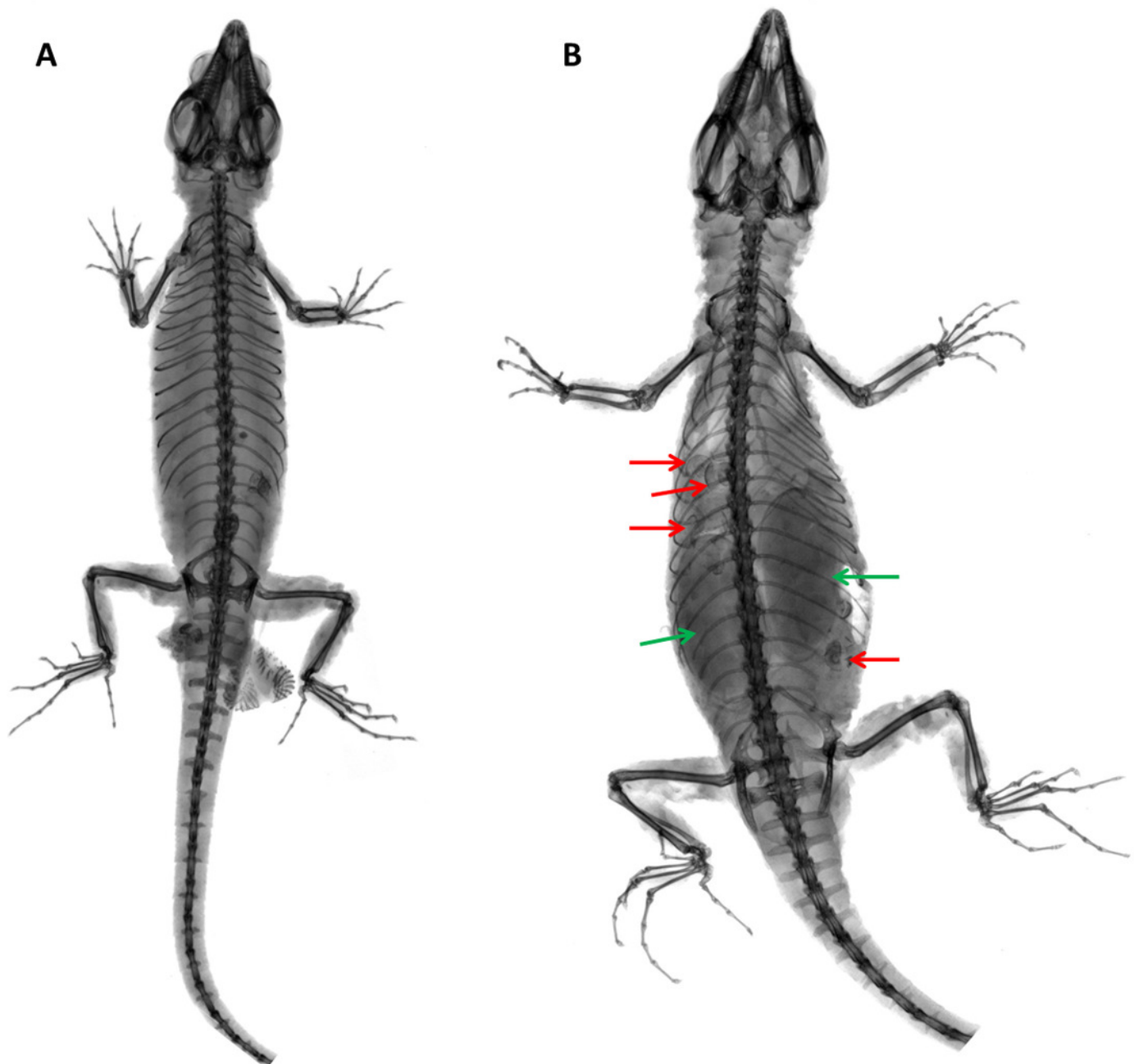
Figure 17

Map of distribution of species of *Echinosaura* in Ecuador.